Title

Aspergillus fumigatus conidial surface-associated proteome reveals factors for fungal evasion and host immunity modulation.

Journal

Nature Microbiology, 9(10)

Authors

Pinzan, Camila
Valero, Clara
de Castro, Patrícia
et al.

Publication Date

2024-10-01

DOI

10.1038/s41564-024-01782-y

Peer reviewed

HHS Public Access

Author manuscript

Nat Microbiol. Author manuscript; available in PMC 2025 April 01.

Published in final edited form as:

Nat Microbiol. 2024 October ; 9(10): 2710–2726. doi:10.1038/s41564-024-01782-y.

Aspergillus fumigatus conidial surface-associated proteome reveals factors for fungal evasion and host immunity modulation

Camila Figueiredo Pinzan[1,11], **Clara Valero**[1,2,11], **Patrícia Alves de Castro**[1], **Jefferson Luiz da Silva**[1], **Kayleigh Earle**[2], **Hong Liu**[3], **Maria Augusta Crivelente Horta**[1], **Olaf Kniemeyer**[4], **Thomas Krüger**[4], **Annica Pschibul**[4], **Derya Nur Cömert**[4], **Thorsten Heinekamp**[4], **Axel A. Brakhage**[4], **Jacob L. Steenwyk**[5], **Matthew E. Mead**[6], **Nico Hermsdorf**[4], **Scott G. Filler**[3,7], **Nathalia Gonsales da Rosa-Garzon**[1], **Endrews Delbaje**[1], **Michael J. Bromley**[2,8], **Hamilton Cabral**[1], **Camila Diehl**[1], **Claudia B. Angeli**[9], **Giuseppe Palmisano**[9], **Ashraf S. Ibrahim**[3,7], **David C. Rinker**[6], **Thomas J. C. Sauters**[6], **Karin Steffen**[6], **Adiyantara Gumilang**[6], **Antonis Rokas**[6], **Sara Gago**[2], **Thaila F. dos Reis**[1], **Gustavo H. Goldman**[1,10]

[1]Faculdade de Ciências Farmacêuticas de Ribeirão Preto, Universidade de São Paulo, Ribeirão Preto, Brazil.

[2]Manchester Fungal Infection Group, Division of Evolution, Infection, and Genomics, Faculty of Biology, Medicine and Health, University of Manchester, Manchester, UK.

[3]Division of Infectious Diseases, Lundquist Institute for Biomedical Innovation at Harbor-UCLA Medical Center, Torrance, CA, USA.

[4]Department of Molecular and Applied Microbiology, Leibniz Institute for Natural Product Research and Infection Biology (Leibniz-HKI) and Institute of Microbiology, Friedrich Schiller University, Jena, Germany.

[5]Howards Hughes Medical Institute and the Department of Molecular and Cell Biology, University of California, Berkeley, Berkeley, CA, USA.

[6]Department of Biological Sciences and Evolutionary Studies Initiative, Vanderbilt University, Nashville, TN, USA.

[7]David Geffen School of Medicine at UCLA, Los Angeles, CA, USA.

Correspondence and requests for materials should be addressed to Antonis Rokas, Sara Gago, Thaila F. dos Reis or Gustavo H. Goldman., antonis.rokas@vanderbilt.edu; sara.gago-2@manchester.ac.uk; thailaf@hotmail.com; ggoldman@usp.br.

[11]These authors contributed equally: Camila Figueiredo Pinzan, Clara Valero.

Author contributions

C.F.P., C.V., P.A.d.C., J.L.d.S., K.E., H.L., O.K., T.K., A.P., D.N.C., T.H., M.A.C.H., J.L.S., M.E.M., N.H., N.G.d.R.-G., E.D., H.C., C.D., C.B.A., G.P., A.S.I., D.C.R., T.J.C.S., K.S., A.G., S.G. and T.F.d.R. performed most of the experiments. A.A.B., S.G.F., M.J.B., A.R. and G.H.G. analysed the data and corrected the manuscript. G.H.G. and C.V. wrote the manuscript and G.H.G. coordinated all the work. All the authors read and edited the manuscript.

Competing interests

J.L.d.S. is a scientific advisor for WittGen Biotechnologies, and an advisor for ForensisGroup Incorporated. A.R. is a scientific consultant for LifeMine Therapeutics, Inc. G.H.G. is a scientific consultant for Innovation Pharmaceuticals Inc. The other authors declare no competing interests.

Additional information

Extended data is available for this paper at https://doi.org/10.1038/s41564–024-01782-y.

Supplementary information The online version contains supplementary material available at https://doi.org/10.1038/s41564–024-01782-y.

[8]Antimicrobial Resistance Network, University of Manchester, Manchester, UK.

[9]Departamento de Parasitologia, Instituto de Ciências Biomédicas, Universidade de São Paulo, São Paulo, Brazil.

[10]National Institute of Science and Technology in Human Pathogenic Fungi, São Paulo, Brazil.

Abstract

Aspergillus fumigatus causes aspergillosis and relies on asexual spores (conidia) for initiating host infection. There is scarce information about *A. fumigatus* proteins involved in fungal evasion and host immunity modulation. Here we analysed the conidial surface proteome of *A. fumigatus*, two closely related non-pathogenic species, *Aspergillus fischeri* and *Aspergillus oerlinghausenensis*, as well as pathogenic *Aspergillus lentulus*, to identify such proteins. After identifying 62 proteins exclusively detected on the *A. fumigatus* conidial surface, we assessed null mutants for 42 genes encoding these proteins. Deletion of 33 of these genes altered susceptibility to macrophage, epithelial cells and cytokine production. Notably, a gene that encodes a putative glycosylasparaginase, modulating levels of the host proinflammatory cytokine IL-1β, is important for infection in an immunocompetent murine model of fungal disease. These results suggest that *A. fumigatus* conidial surface proteins are important for evasion and modulation of the immune response at the onset of fungal infection.

Pulmonary fungal diseases caused by the environmental mould *Aspergillus fumigatus* lead to important morbidity and mortality. In patients with weakened lung defences arising from immunosuppression (a chronic respiratory condition) or a previous respiratory infection, asexual spores (referred to as conidia) of *A. fumigatus* can evade the lung defences, germinate and cause disease[1]. However, our understanding of what makes *A. fumigatus* a successful pathogen compared with other species remains incomplete. Current evidence suggests that several different *Aspergillus* species, including *A. fumigatus*, probably independently evolved the ability to cause human disease[2] (Fig. 1a), raising the idea that expression of specific proteins on conidia contributes to species-specific virulence properties.

The early stages of disease, marked by the interaction between the inhaled conidia and the host, may prove insightful for unravelling *A. fumigatus* pathogenicity. Among studies of other microbial pathogens, there has been an increasing focus on conidial surface protein characterization since they mediate the first encounter with the host immune system. The conidial cell wall comprises a β−1,3-glucan and chitin body, which is covered by rodlet and melanin layers, where proteins are anchored[3,4]. Surface proteins play pivotal roles in morphogenesis, resistance to environmental stressors, substrate adherence and virulence[5]. The hydrophobin RodA is a key component of the rodlet layer and is essential for cell wall physical resistance and permeability, preventing immune recognition[6,7]. Another conidial surface protein, CcpA, is essential to maintain the correct surface structure and prevent immune recognition[8]. HscA has been demonstrated to anchor human p11 on phagosomal compartments in epithelial cells, rewiring vesicular trafficking to the non-degradative pathway, facilitating the escape of conidia[9]. Other studies aimed to identify potential vaccine candidates, allergens and biomarkers for diagnosis[5,10,11].

Due to the importance of conidia for disease, several previous studies have investigated conidial surface proteins[5,8,10,12,13], but a comprehensive examination of their contribution to pathogenicity in *A. fumigatus* and closely related species is lacking. Here we analysed the conidial surface proteome of *A. fumigatus* and three closely related species: (1) *Aspergillus lentulus*, which is a cryptic pathogen[14]; (2) *Aspergillus oerlinghausenensis*, the closest known relative of *A. fumigatus*, which is azole resistant but non-pathogenic[15,16]; and (3) *Aspergillus fischeri*, a close relative of *A. fumigatus* that is less virulent in several animal models and rarely causes disease in humans[17] (Fig. 1a).

Results

A. fumigatus has increased virulence and cytokine production

We comparatively analysed the capacity of reference strains of *A. fumigatus* A1163, *A. oerlinghausenensis* CBS 139183^T, *A. fischeri* NRRL 181 and *A. lentulus* CNM-CM6069 to infect susceptible hosts in vivo and macrophages in vitro. In a chemotherapeutic BALB/c murine model of invasive pulmonary aspergillosis (IPA), *A. fumigatus* strain A1163 was more virulent than *A. fischeri*, *A. oerlinghausenensis* and *A. lentulus* strains ($P < 0.005$, Fig. 1b) and killed all mice after 5 days post infection (d.p.i.).

In bone-marrow-derived macrophages (BMDMs), *A. fumigatus* A1163 conidia were slightly more engulfed than conidia from *A. lentulus*, *A. oerlinghausenensis* or *A. fischeri* reference strains, yet *A. fumigatus* A1163 conidia survived BMDM co-incubation more readily than conidia from the *A. lentulus*, *A. oerlinghausenensis* and *A. fischeri* reference strains (Fig. 1c,d). *A. fumigatus* conidia are recognized by macrophages and are intracellularly degraded by the endocytic pathway through the fusion of conidia-containing phagosomes and lysosomes, forming an acidic phagolysosome (PL)[18]. Melanin can facilitate evading this mechanism, as the *A. fumigatus* Δ*pksP* mutant (which lacks a key enzyme involved in melanin biosynthesis) induces higher levels of PL acidification than the corresponding wild-type strain ATCC46645 (Fig. 1e). There are no differences in PL acidification in *A. fumigatus*, *A. fischeri*, *A. oerlinghausenensis* and *A. lentulus* (Fig. 1e). In contrast, *A. fumigatus* conidia induces higher levels of cytokines TNF-α, IL-6, IL-1β and 1L-18 in BMDMs than the other three species (Fig. 1f–i). *A. fumigatus* strain A1163 and *A. lentulus* induced production of inflammasome IL-1β and IL-18, while *A. fischeri* strain NRLL 181 and *A. oerlinghausenensis* conidia led to the production of lower levels of TNF-α than *A. fumigatus* and *A. lentulus* conidia (Fig. 1f–i).

There are no differences in conidia internalization by A549 epithelial cells between *A. fumigatus* and *A. fischeri*, and *A. fumigatus* and *A. lentulus*; however, *A. oerlinghausenensis* is different from all the three species (Fig. 1j). *A. fumigatus* and *A. fischeri* cause comparable damage to A549 epithelial cells, while *A. lentulus* causes more damage than *A. fumigatus*. *A. oerlinghausenensis* causes less damage than the three other species (Fig. 1k).

Taken together, these results indicate that *A. fumigatus* A1163 is more virulent in a chemotherapeutic murine model of IPA compared with closely related species and can overcome phagocytic activities by BMDMs.

A. fumigatus is phenotypically distinct from *Afi*

We extended the number of strains to eight *A. fumigatus* clinical isolates and eight environmental strains from *A. fischeri* (Supplementary Table 1). We evaluated 29 phenotypic parameters, aiming to compare radial growth, biofilm formation, induction of inflammatory mediators and host–fungus interactions (see Supplementary Tables 2–7). Principal component analysis of data from all 29 phenotypes showed that *A. fumigatus* is phenotypically distinct from *A. fischeri* (Extended Data Fig. 1a). Analysis of each of the investigated phenotypes showed that 12 of the 29 phenotypes are statistically different between *A. fumigatus* and *A. fischeri* (Extended Data Fig. 1b and Supplementary Table 7). Our results indicate that although *A. fumigatus* and *A. fischeri* are globally phenotypically distinct from each other, there is high heterogeneity in several phenotypic traits (Fig. 1e,h, Extended Data Fig. 1b and Supplementary Tables 3–7), suggesting that variability within species is similar to or exceeds interspecies variability for some phenotypic traits. However, it is important to note that immune-mediated or host–fungal interaction phenotypes (cytokine induction, killing assays, A549 endocytosis and dectin staining) do not appear to contribute to global species-specific differences. The difference largely maps to growth properties.

Sixty-two proteins were detected on the conidial surface

Conidial surface proteins may underlie variation in host recognition. To test this hypothesis, we conducted a trypsin-shaving proteomic analysis and identified proteins that were uniquely detected on the *A. fumigatus* conidial surface. Samples of resting (0 h) and swollen (4 h, 37 °C) conidia from *A. fumigatus*, *A. fischeri*, *A. oerlinghausenensis* and *A. lentulus* (Fig. 2a) were collected and processed for LC–MS/MS analysis as described in ref. 5 (Fig. 2b,c). Extended Data Fig. 2 and Supplementary Table 9 summarize the total number of proteins for each species.

Comparative analyses of the surfome revealed 62 conidial surface proteins exclusively detected in *A. fumigatus* conidia. The 62 genes encoding these proteins are present in all four species. Fifty-six of the genes encoding these proteins are shared by all 206 *A. fumigatus* isolates, whereas 6 (AFUB_028320, AFUB_039180, AFUB_045200, AFUB_050510, AFUB_069520 and AFUB_094680) were more variable, belonging to the accessory pangenome[19].

Functional categorization (https://fungidb.org) showed that most genes encode enzymes involved in biological processes such as cell wall modification, metabolism, cell signalling and secondary metabolite biosynthesis (Fig. 2c and Supplementary Table 10). However, more than a third of the proteins identified as part of the *A. fumigatus*-specific conidial surfome had unknown functions (Fig. 2c). Thirty-one of the 62 proteins were predicted to have a signal peptide cleavage site, while only 2 had high probability (>99%) of harbouring a glycosylphosphatidylinisotol-anchoring signal (Supplementary Table 10). We examined the expression of these 62 genes in an RNAseq dataset that describes gene modulation during conidial germination[20] (Fig. 2d). About 27% of the 62 genes whose protein products are detected only in *A. fumigatus* (16 genes) did not change their gene expression during the first 16 h of germination, while 33% (21 genes) had increased expression during the 2–16 h

germination window (Fig. 2d). About 24% of the surfome genes (15 genes) were expressed late, while 16% (10 genes) were expressed early (Fig. 2d).

To confirm the localization of these proteins, functional strains expressing four of these proteins fused to green fluorescent protein (GFP) were constructed (Supplementary Fig. 1a–i). All these GFP strains, but not the wild-type strain, displayed extremely low (except for AFUB_100320:GFP that shows a very strong signal) GFP fluorescence signal near the surface of resting and swollen conidia but not in germlings (Supplementary Fig. 1a–i, and Tables 9 and 10).

There are five previous studies reporting the identification of *A. fumigatus* conidia-associated proteins[5,8,10,12,13]. In these studies, various techniques were used to extract conidial proteins, such as elution with NaCl, HF-pyridine or SDS buffer, trypsin-shaving or mild alkaline buffer in the presence of ß-1,3-glucanase. In total, there are 1,221 different proteins identified in all these manuscripts. The results of protein extraction are quite variable and none of our conidia-associated proteins are present in all five datasets. However, 64.5% of the uniquely conidia-detected proteins identified in our work (40 of 62 proteins) are present in at least one other dataset (Supplementary Table 11).

Mutant analysis of 42 genes encoding conidial proteins

We were unable to construct deletion mutants for 20 of the 62 *A. fumigatus*-specific genes that were not present in the COFUN homozygous library[21] (Supplementary Table 12). Taking into consideration a 30% increase or decrease compared with the parental strain (A1163), we observed the following mutant phenotypes. Growth rates on solid minimal medium (MM) at 37 °C revealed no mutants with growth defects compared with the parental A1163 strain. None of the mutants exhibited increased sensitivity to heat (44 °C) or oxidative stress caused by H_2O_2 (Fig. 2e and Supplementary Table 10). However, ΔAFUB_058080 was found to be more sensitive than the A1163 wild-type strain to the cell wall stressor Congo Red (CR). Germination rates for 33 mutants behaved similarly to the A1163 reference strain. The remaining deletion strains could be differentiated into two groups: (1) 4 mutants showed slow germination and (2) 5 mutants showed fast germination (Fig. 2f and Supplementary Table 10). We performed both the biofilm dye Crystal Violet (CV) assay (for measuring adhesion) and adhesion to A549 lung cells for resting and swollen stages. Notable differences were observed for 9 strains that displayed reduced adhesion properties in comparison with A1163 (Fig. 2g and Supplementary Table 10). In vivo adhesion on A549 pulmonary epithelial cells revealed 7 mutants with increased adhesion, and 2 mutants with decreased adhesion (Fig. 2h and Supplementary Table 10).

Calcofluor white (CFW) staining revealed a group of 8 deletion strains that exhibited lower chitin content than the wild-type strain, and wheat germ agglutinin (WGA) labelling revealed a set of 11 mutant strains that showed higher chitin exposure (Fig. 2i and Supplementary Table 10). Using a dectin-based immunofluorescent assay, we identified 1 and 3 mutants with higher and lower β-D-glucan exposure, respectively, compared with the A1163 wild-type strain (Fig. 2i and Supplementary Table 10). Finally, only one mutant showed altered hydrophobicity properties compared with the A1163 wild-type strain (Extended Data Fig. 3 and Supplementary Table 10).

Taken together, these results suggest that *A. fumigatus* conidial surface-associated proteins are also involved in the correct assembly of the cell wall and have an important role in combatting stress and adhering to surfaces.

Surfome proteins are involved in host–pathogen interactions

Assuming once more a 30% increase or decrease compared with the parental strain (A1163), we identified 18 *A. fumigatus* genes encoding surface proteins that contribute to survival to macrophage killing (9 null strains were more susceptible to macrophage killing and 9 were more resistant) (Extended Data Fig. 4a and Supplementary Table 10). Twenty-seven *A. fumigatus* genes encoding for surface proteins were important for epithelial cell invasion (3 mutants were more efficiently taken up by the epithelial cells, while 24 exhibited defects in cell invasion) (Extended Data Fig. 4b and Supplementary Table 10).

There is no correlation between macrophage survival and epithelial cell invasion (Extended Data Fig. 4c), but 14 *A. fumigatus* mutants of genes encoding surfome proteins were identified to be involved in both killing and invasion (Extended Data Fig. 4a,b and Supplementary Table 10). The capacity of the null mutants to induce epithelial cell damage was also evaluated, with 3 strains producing less damage than the A1163 strain and only 1 triggering higher cell toxicity (Extended Data Fig. 4d and Supplementary Table 10).

Our comparative data indicate that *A. fumigatus* induces a stronger immune response in BMDMs (Fig. 1e–h). Thus, phenotypic analyses were carried out using RAW 264.7 murine macrophages immortalized cell lines and to confirm observations, we utilized primary BMDMs. We observed an increased IL-1β production in 11 mutants and decreased production in 3 mutants (Extended Data Fig. 4f and Supplementary Table 10). TNF-α production was importantly increased in 1 mutant and decreased in 3 mutants (Extended Data Fig. 4f and Supplementary Table 10). Only the ΔAFUB_065340 (encoding a zinc-containing alcohol dehydrogenase) mutant had ~80% reduced lactate dehydrogenase (LDH) activity and decreased BMDMs survival.

We identified two clusters of genes with higher expression in RNAseq datasets of *A. fumigatus* exposed toanimal cells or invasive aspergillosis conditions (https://cparsania.shinyapps.io/FungiExpresZ/; Supplementary Fig. 2a and Table 13). These two clusters contain 22 genes, 11 of which are also among the 62 encoding *A. fumigatus* uniquely detected genes, suggesting that the corresponding protein products of these 11 genes could be important for host–pathogen interactions and the establishment of infection (Supplementary Fig. 2b,c and Table 10). Furthermore, 7 of the 62 *A. fumigatus* uniquely detected genes were among the 1,700 genes whose evolutionary rate differed between pathogenic and non-pathogenic species from *Aspergillus* section Fumigati[22] (Supplementary Fig. 2d and Table 14).

These results suggest that some of the proteins identified as uniquely detected in the *A. fumigatus* surfome, but which are absent from the conidia of the three other closely related species, are important for mediating host interactions and eliciting cytokines, and are modulated at the transcriptional level in the presence of animal cells.

Characterization of a glycosylasparaginase null mutant

We prioritized the mutants that elicited increased IL-1β production (Supplementary Fig. 2e and Table 10) and displayed differences in gene evolutionary rates in pathogenic and non-pathogenic species. This prioritization scheme led to the decision to start by characterizing the ΔAFUB_059140 mutant (here named Δ*aspA*). We constructed a second independent Δ*aspA* mutant and both independent *aspA* null mutants display the same phenotypes (Extended Data Fig. 5). The *aspA* gene encodes a putative glycosylasparaginase that catalyses the hydrolysis of N4-(β-*N*-acetyl-D-glucosaminyl)-L-asparagine, yielding as products *N*-acetyl-β-glucosaminylamine plus L-aspartate (Supplementary Fig. 2e). This activity cleaves the GlcNAc-Asn bond that links oligosaccharides to asparagine in N-linked glycoproteins, playing a major role in the degradation of glycoproteins (http://pfam-legacy.xfam.org/; PF01112). AspA is distributed among several fungal classes, including in Eurotiomycetes, Dothideomycetes and Sordariomycetes, three classes that contain most of the plant and animal pathogens (Supplementary Fig. 2f). The Δ*aspA* mutants are more phagocytosed by BMDMs than the wild type (Fig. 3a), have increased percentage of adherent conidia on the surface of BMDMs, decreased cell viability as measured by chitin content (CFW fluorescence), and decreased metabolic activity as measured by (3-[4,5-dim ethylthiazol-2-yl]-2,5 diphenyl tetrazolium bromide) (MTT) assay (Fig. 3a–c). The increased expression of IL-1β triggered by the Δ*aspA* mutants is dependent on the viability of their conidia since UV-killed conidia did not trigger IL-1β and TNF-α compared with the wild-type strain (Fig. 3d). BMDMs have increased production of reactive oxygen species (ROS) when in the presence of the Δ*aspA* mutant for 8 h, suggesting that this mutant is either not able to cope with ROS detoxification at this timepoint or induces increased ROS production (Fig. 3e). The Δ*aspA* mutant has the same ability as the wild type to evade phagolysosome acidification (Fig. 3f). Transwell migration assays showed that most of the increased production of IL-1β by *aspA* mutants needed contact with BMDMs (Fig. 3g). In contrast, TNF-α production was equally dependent on contact for either the wild type or Δ*aspA* mutants (Fig. 3h). When exposed to alveolar macrophages, the Δ*aspA* mutants led to increased production of IL1-β, IL-6 and IL-18 but not TNF-α, and reduced viability compared with the wild-type strain (Extended Data Fig. 6).

Taken together, these results suggest that AspA is important for BMDMs and alveolar macrophage phagocytosis and viability of *A. fumigatus* conidia, and that AspA can modulate cytokine production by direct contact of the conidia with BMDMs or alveolar macrophages.

AspA is important for establishment of virulence

A. fumigatus Δ*aspA* mutants have the same virulence as the wild type in a chemotherapeutic murine model, but they are less virulent in an immunocompetent murine model as measured by fungal burden (Fig. 4a,b). We measured the production of cytokines TNF-α, IL-1β, IL-18, IL-12, INF-ϒ and IL-6, and the chemokine CXCL-1 in the lung homogenates of the immunocompetent model infected by wild type and Δ*aspA* mutants (Fig. 4c–i). The lack of AspA caused increased production of proinflammatory cytokines and CXCL-1 that acts as a chemoattractant for several immune cells and that is induced upon *A. fumigatus* lung infection[23]. However, Δ*aspA* did not elicit increased neutrophil migration in the murine

lungs compared with the wild-type strain (Fig. 4j,k and Extended Data Fig. 7). Our results indicate that AspA is important for attenuating inflammatory responses during the early steps of *A. fumigatus* infection in the lungs.

Characterization of heterologously expressed glycosylasparaginase

We heterologously expressed AspA in *Pichia pastoris* (Extended Data Fig. 8a). Incubation of BMDMs with increasing AspA concentrations had no impact on their LDH activity (Fig. 5a). AspA at 0.2 μg or 2 μg decreased BMDMs viability by ~1 and 10%, respectively, while dimethylsulfoxide (DMSO) decreased BMDMs viability by 80% (Fig. 5b). AspA Scan modulate IL-1β and TNF-α production by using different AspA concentrations in a linear dose-response relationship (Fig. 5c,d). Cytokine induction by AspA is not related to its glycosylation since exposure of AspA to peptide:*N*-glycosidase F (PNGase F)[24,25] did not abolish this induction (Extended Data Fig. 8b). The low GFP expression of AspA:GFP did not allow us to perform protein localization studies (Supplementary Fig. 1j,k). AspA:GFP fused with the strong constitutive *gpdA* promoter from the glyceraldehyde-3-*P*-dehydrogenase gene allowed us to observe fluorescence of the AspA:GFP near the surface of resting and swollen conidia, but not in the germlings (Supplementary Fig. 1l,m). AspA exhibited asparaginase activity (Fig. 5e) and its inactivation by boiling for 5 min decreased IL-1β production by ~50% (Fig. 5f). Surprisingly, AspA was also able to induce TNF-α production and AspA inactivation decreased its accumulation by 30% (Fig. 5f). We also observed that AspA modulated IL-1β, IL-6, IL18 and TNF-α release by alveolar macrophages and that AspA inactivation by boiling also reduced cytokine accumulation (Extended Data Fig. 6). Next, we investigated whether previous (by 8 h) or concomitant exposure of BMDMs to 2 μg of AspA and conidia could change conidial viability (Fig. 5h). Both treatments increased conidial viability by ~20%, indicating that AspA contributes to conidial viability (Fig. 5h).

Taken together, these results suggest that AspA modulates cytokine levels of both BMDM and alveolar macrophages, and increases conidial viability in the presence of BMDMs.

Proteomic profiling of BMDMs exposed to AspA

We incubated BMDMs in the presence of 0.2 μg AspA for 24 h and identified the proteins by mass spectrometry (Supplementary Table 10). Differentially produced proteins are defined as those with a minimum of 2-fold change in protein abundance ($\log_2 FC \geq 1.0$ and ≤ -1.0; false discovery rate (FDR) of 0.05) compared with BMDMs under the equivalent conditions. We observed 101 upregulated and 259 downregulated proteins in the BMDMs exposed to AspA (Fig. 6a,b and Supplementary Table 15).

We then used the Reference Database of Immune cells (http://refdic.rcai.riken.jp/document.cgi) for Gene Ontology (GO) and Kyoto Encyclopedia of Genes and Genomes (KEGG) pathway enrichment analysis of distinct biological functions of the shared and specific proteomic differences. The BMDM proteins downregulated in the presence of AspA are involved in: (1) cell redox homoeostasis, metabolic process, oxidation reduction and response to oxidative stress; (2) carbohydrate metabolism, such as pentose-phosphate shunt, tricarboxylic acid cycle and glycolysis/gluconeogenesis; (3) protein synthesis; (4)

pyruvate metabolism and (5) ubiquitin-dependent protein catabolism (Fig. 6c,d). In contrast, protein transport, vesicle-mediated transport, mRNA processing and metabolic processes were upregulated (Fig. 6c). We also manually detected the downregulation of 18 proteins specifically related to the modulation of the innate immune and lysosomal functions (Supplementary Tables 15 and 16). Examination of the general mouse functional protein association network, retrieved from STRING (https://string-db.org) showed that 15 of these 18 proteins have functional associations, suggesting that AspA impacts specific protein interaction networks (Fig. 6e).

Taken together, our results suggest that AspA modulates several BMDM metabolic pathways specifically affecting the abundance of proteins important for immune function.

Discussion

A. fumigatus is a prominent human fungal pathogen that infects and frequently kills hundreds of thousands of individuals yearly. Most other closely related species, on the other hand, are not pathogenic[2,16,26]. The observed pathogenicity spectrum cannot be solely explained by changes in species ecologies or ascertainment bias, suggesting that the repeated evolution of *Aspergillus* pathogenicity has, at least in part, a genetic foundation[2]. Conidia are the first fungal structure that encounters the host. In immunocompetent hosts, conidia are cleared and do not affect host health. There are several mechanisms of conidial and germling recognition but also evasion based on melanin and polysaccharides, such as β−1,3-glucan, and galactosaminogalactan secreted by the fungus during conidial germination and hyphal formation, and immunomodulation based on chitin, present on the conidial surface[23]. Although the importance of protein effectors for pathogenesis and virulence has been extensively described in plant fungal pathogens, there are very few reports about conidial surface proteins or protein effectors in human fungal pathogens[6,8,9,27–29].

Here we compared *A. fumigatus* conidial surface proteins with those of two closely related non-pathogenic species, *A. fischeri* and *A. oerlinghausenensis*, and one pathogenic species, *A. lentulus*. Using this approach, we identified 62 *A. fumigatus* uniquely conidia-detected surface proteins in our reference strain A1163 and were able to delete 42 of them. These *A. fumigatus* detected surface proteins could be potential surface proteins or protein effectors that modulate different aspects of virulence and pathogenicity or alternatively new genetic determinants important for maintaining the correct conidial structure allowing attachment to host surfaces or preventing immune recognition. Several of them affect interaction with host cells since they modulate survival in the presence of macrophages, invasion and/or damage to epithelial cells, and cytokine production. This collection of genes and mutants provides an opportunity for the characterization of genetic determinants important for *A. fumigatus*–host interaction.

We focused on one of these genetic determinants, a gene encoding a glycosylasparaginase, named AspA. To our knowledge, this is presumably the first characterized fungal glycosylasparaginase. Homologues of this gene are not present in *Saccharomyces cerevisiae* and when mutated in humans (AGA gene), cause the most frequent type of recessively inherited lysosomal storage disease named aspartylglucosaminuria (AGU)[27]. AGU is a

disorder related to degradation of glycoproteins. Carbohydrate moieties are typically found in glycoproteins and are linked to the protein moiety by an N-glycosidic bond formed by the amino acid L-asparagine and the monosaccharide *N*-acetylglucosamine. The lysosomal resident enzyme glycosylasparaginase, which cleaves the N-glycosidic link between the L-asparagine and *N*-acetylglucosamine moieties of GlcNAc-Asn, is lacking in AGU. This enzyme deficiency causes a buildup of undegraded aspartylglucosamine and several other glycoasparagines, that is, glycoconjugates having an L-asparagine moiety attached to the carbohydrate chain, in the affected person's tissues and body fluids[30–32].

As far as we know, there is no previous information about the involvement of glycosylasparaginases in bacterial and fungal pathogenesis. However, there are several reports about possible roles played by asparaginases in bacterial virulence[33–38], but not in fungal virulence. *A. fumigatus* has two putative glycosylasparaginases (AFUB_059140, which is described here, and AFUB_021340, none of which has a putative signal peptide) and two asparaginase encoding genes (AFUB_003170 and AFUB_051450, with and without a putative signal peptide, respectively). It remains to be investigated whether these genes are also important for *A. fumigatus* virulence.

The Δ*aspA* mutants are more phagocytosed and killed than the wild type, elicit more ROS production and require contact with BMDMs to have increased IL-1β production, but have identical percentages of acidification of the phagolysosomes. These results suggest that AspA has a role in earlier or later steps after the formation of phagolysosomes. AspA is important for the establishment of infection in an immunocompetent mouse model but not in the chemotherapeutic mouse model, and the lack of AspA also plays an important role in modulating proinflammatory cytokines in vivo. The lack of AspA causes increased production of proinflammatory cytokines and CXCL-1 that acts as a chemoattractant for several immune cells, especially neutrophils, and it has already been observed to be induced upon *A. fumigatus* lung infection[22]. Our results indicate that AspA is important for modulating the inflammatory response but not the migration of neutrophils upon *A. fumigatus* infection of the lungs.

We also investigated AspA through its heterologous expression and its influence on cytokine production and macrophage metabolism. The human glycosylasparaginase has both deglycosylation and asparaginase activities[38], and we were able to detect asparaginase activity for the *A. fumigatus* AspA protein. When BMDMs were exposed to AspA, there was a dramatic change in its proteomic profiling, with decreased cell redox, carbohydrate and pyruvate metabolism, and protein biosynthesis, suggesting that AspA affects the aerobic metabolism and ROS production of BMDMs, and decreases the expression of proteins important for ROS production, such as neutrophil cytosol factor 1 (Ncf1), a cytosolic subunit of neutrophil NADPH oxidase. It has been previously shown that patients with hypersensitivity pneumonitis, a rare initial presentation in chronic granulomatous disease, carry mutations in NCF1 and NCF2 genes and are more susceptible to an invasive pulmonary aspergillosis infection caused by *A. fumigatus*[37]. We also observed that exposure of BMDMs to AspA decreased the production of several lysosomal proteases, cathepsins, important for protein degradation.

Upon conidial phagocytosis, phagosomes are fused with lysosomes resulting in functional phagolysosomes that are an integral part of a degradative pathway that kills and destroys[39]. AspA might also be important for escaping phagolysosomal killing. An attractive model for the AspA mechanism of action could be that upon conidial phagocytosis, AspA is already interacting with proteins at the macrophage surface, deglycosylating asparagine residues and modifying protein activity. Upon conidial phagocytosis and during the formation of phagolysosomes, AspA remains active in the phagolysosome, eventually deglycosylating asparagine residues affecting conidial survival. It is possible that after partial conidial destruction, AspA remains active in the host lysosome, affecting glycosylation metabolism in the cell and consequently allowing some conidia to survive. *A. fumigatus* conidia can persist for some time in the phagosomes of immune cells and epithelial cells[18,40–42]. AspA could affect the host's membrane trafficking system or redirect the conidia-containing phagosomes towards exocytosis and release of conidia. Different aspects of our proposed model remains to be investigated.

Methods

Fungal strains

All strains included in this work are listed in Supplementary Table 1. Knockout mutant strains belong to the Manchester Infection Fungal Group (MFIG) collection and were constructed as described in ref. 20. GFP fusion replacement cassettes were constructed by in vivo recombination in *S. cerevisiae*, as previously described[43,44].

Proteome analyses and BMDM protein extraction

Freshly collected conidia of *A. fumigatus* A1163, *A. oerlinghausenensis* CBS 139183^T, *A. fischeri* NRRL 181 and *A. lentulus* CNM-CM6069 were cultivated on potato dextrose agar (PDA) at 37 °C for 8 days, and immediately collected and processed. Resting conidia from this suspension or 4 h germinated conidia in liquid PDA medium (swollen conidia) were used for the trypsin-shaving experiments. Conidia (1×10^9) of each species strain in three biological replicates were washed twice with 25 mM ammonium bicarbonate (AB) and centrifuged at 1,800 × *g* for 10 min. Conidia were resuspended in 800 µl of 25 mM AB and incubated with 5 µg trypsin (MS approved, Serva) for 5 min at 37 °C. Cell suspensions were immediately passed through 0.2 µm syringe filters (cellulose acetate, Sartorius) to separate conidia from the digestion buffer, followed by washing the filters with 200 µl of 25 mM AB. Subsequently, 10 µl of 90% (v/v) formic acid was added to the cell-free solution to stop the proteolytic digestion. Samples were evaporated to dryness in a vacuum concentrator (Eppendorf), resuspended in 30 µl of 2% (v/v) acetonitrile (ACN) and 0.05% (v/v) trifluoroacetic acid, centrifuged for 15 min at 14,000 × *g* through 10 kDa molecular weight cut-off filters (modified PES, VWR), and transferred into HPLC vials.

LC−MS/MS analysis was performed on an Ultimate 3000 RSLC nano instrument coupled to a QExactive HF mass spectrometer (Thermo Fisher) as described previously[5]. Tryptic peptides were trapped for 4 min on an Acclaim Pep Map 100 column (2 cm × 75 µm, 3 µm) at a flow rate of 5 µl min^{-1}. Peptides were further separated on an Acclaim Pep Map column (50 cm × 75 µm, 2 µm) using a binary gradient of eluents A (0.1% (v/v) formic acid

in H_2O) and B (0.1% (v/v) formic acid in 90:10 (v/v) ACN/H_2O): 0–4 min at 4% B, 5 min at 8% B, 20 min at 12% B, 30 min at 18% B, 40 min at 25% B, 50 min at 35% B,57 min at 50% B, 62–65 min at 96% B, 65.1–90 min at 4% B. Positively charged ions were generated by a Nanospray FlexIon Source (Thermo Fisher) using a stainless steel emitter with 2.2 kV spray voltage. Ions were measured in the full MS/data-dependent MS2 (Top15) mode. Precursor ions were scanned at m/z 300–1,500, a mass resolution of 60,000 full width at half maximum (FWHM), an automatic gain control (AGC) target of 1×10^6, and a maximum injection time (maxIT) of 100 ms. Precursor ions were isolated with a width of m/z 2.0. Fragment ions generated in the higher-energy collisional dissociation cell at 30% normalized collision energy using N_2 gas were scanned at 15,000 FWHM, an AGC target of 2×10^5 and a maxIT of 80 ms. Dynamic exclusion was set to 25 s.

The MS/MS data were searched against the FungiDB databases of *A. fumigatus* Af293 and *A. fischeri* NRRL_181, the NCBI database of *A. lentulus* and the JGI database of *A. oerlinghausenensis* (all downloaded on 27 October 2020) using Proteome Discoverer 2.4 and the algorithms of Mascot 2.4.1, Sequest HT, MS Amanda 2.0 and MS Fragger 3.0. Two missed cleavages were allowed for the tryptic digestion. The precursor mass tolerance was set to 10 ppm and the fragment mass tolerance was set to 0.02 Da. Modifications were defined as dynamic Met oxidation, protein N-term acetylation and/or loss of methionine. A strict FDR < 1% (peptide and protein level) and a search engine score of >30 (Mascot), >4 (Sequest HT), >300 (MS Amanda) or >8 (MS Fragger) were required for positive protein hits. The Percolator node of PD2.4 and a reverse decoy database were used for q-value validation of spectral matches. Only rank 1 proteins and peptides of the top scored proteins were counted (Supplementary Table 9).

The infected macrophage proteome analysis was performed through lysis in 8 M urea in 25 mM AB containing protease inhibitor cocktail using a probe tip sonicator: 40% amplitude for 3 cycles of 10 s and intervals of 10 s. After sonication, samples were centrifuged, the supernatant was transferred to a new tube and quantified using Bradford reagent. Proteins were reduced with 10 mM dithiothreitol for 30 min at 30 °C, alkylated with 40 mM iodoacetamide for 40 min at room temperature in the dark and overnight digested with trypsin at an enzyme to protein ratio of 1:50. The tryptic peptides were desalted with Oasis HLB Cartridges (Waters) according to manufacturer instructions, dried down by speed vacuum, and then resuspended in 0.1% formic acid. LC–MS/MS analysis was performed in an EASY-nLC system (Thermo Scientific) coupled to an LTQ-Orbitrap Velos mass spectrometer (Thermo Scientific). Peptides were separated on a C18 PicoFrit column (C18 PepMap, 75 μm id × 10 cm, 3.5 μm particle size, 100 Å pore size; Thermo Fisher) using a gradient of A and B buffers (buffer A: 0.1% formic acid; buffer B: 95% acetonitrile, 0.1% formic acid) at a flow rate of 300nl min^{-1}: from 2% to 30% B over 80 min and from 30% to 90% B over 5 min. The LTQ-Orbitrap Velos was operated in positive ion mode with data-dependent acquisition. The full scan was obtained in the Orbitrap with an AGC target value of 1×10^6 ions and a maximum fill time of 500 ms. Each precursor ion scan was acquired at a resolution of 60,000 FWHM in the 400–1,500 m/z mass range. Peptide ions were fragmented by collision induced dissociation MS/MS using a normalized collision energy of 35. The 20 most abundant peptides were selected for MS/MS and dynamically excluded during 30 s. All raw data were accessed in the Xcalibur software (Thermo Scientific). For

protein identification, raw data were processed using MaxQuant software v.1.5.3.8. The MS/MS spectra were searched against a protein database composed of *A. fumigatus* and human sequences with the addition of common contaminants with a tolerance level of 4.5 ppm for MS and 0.5 Da for MS/MS. Trypsin was selected as a specific enzyme with a maximum of two missed cleavages. Carbamidomethylation of cysteine (57.021 Da) was set as a fixed modification, and oxidation of methionine (15.994 Da), deamidation NQ (+0.984 Da) and protein N-terminal acetylation (42.010 Da) were set as variable modifications. Peptide-spectrum matches (PSMs), peptides and proteins were accepted at FDR less than 1%.

Multivariate statistical analyses were performed on the protein groups using the label-free quantification (LFQ) results. The analyses were conducted using the LFQ-Analyst web platform[45] with default parameters, including a *P*-value cut-off of 0.05 and a $\log_2$ fold change cut-off of 1.

For protein identification, raw data were processed using MaxQuant software v.1.5.3.8. The MS/MS spectra were searched against a protein database composed of human sequences with the addition of common contaminants with a tolerance level of 4.5 ppm for MS and 0.5 Da for MS/MS. Trypsin was selected as a specific enzyme with a maximum of two missed cleavages. Carbamidomethylation of cysteine (57.021 Da) was set as a fixed modification, and oxidation of methionine (15.994 Da), deamidation NQ (+0.984 Da) and protein N-terminal acetylation (42.010 Da) were set as variable modifications. Proteins and peptides were accepted at FDR less than 1%.

Glycosylasparaginase heterologous expression

The synthetic asparaginase gene (AFUB_059140) cloned in the expression vector pPICZαA (Invitrogen) was synthesized by Genescript. The vector has optimized codons for the expression of *Komagataella phaffii* and the α factor secretion signal in the N-terminal portion, and Zeocin resistance gene. The plasmid obtained was propagated in competent *Escherichia coli* (DH10β) cells (Thermo Fisher) resistant to Zeocin. The purified plasmid was linearized using the Anza 24 MssI restriction enzyme (Invitrogen), purified again and transformed into competent *K. phaffii* (KM71H) by electroporation (1.5 kV, 25 mF and 200 Ω) in a 0.2 μm cuvette using an electroporator (MicroPulser Electroporator, Bio-Rad). The recombinant strain was selected, cultivated and induced to express the rAsparaginase protein following the EasySelect *Pichia* Expression Kit manual (Invitrogen). After 120 h of induction with 1% (v/v) methanol, the material was centrifuged (5,000 × *g*, 45 min at 4 °C) and the supernatant was filtered through a 0.22 μm filter.

The filtered material was dialysed against 50 mM Bicine buffer (pH 8.5) and subjected to anion exchange purification. The Mono Q 5/50 GL column (GE Healthcare) was equilibrated with 50 mM Bicine buffer (pH 8.5) and the enzyme eluted with 180 mM NaCl. Protein integrity and sample purity were confirmed by running a 12% SDS–PAGE[46]. Purified protein fractions were dialysed against 1X phosphate-buffered saline (PBS, pH 7.4) using the Vivaspin 10 kDa centrifuge system (Sartorius). Protein quantification was performed in a spectrophotometer at 280 nm and the assays were performed with the enzyme at a concentration of 5.88 μM.

AspA phylogenetic analysis

To visualize the distribution of the glycosylasparaginase gene presence among fungi, the AspA amino acid sequence (AFUB_059140) was used for a BLAST search[47] against the NCBI RefSeq database[48]. The 687 sequences found were aligned using MAFFT (v.7.508)[49] to infer a maximum likelihood phylogenetic tree using IQ-TREE (v.1.7)[50] with the substitution model JTT+I+G4, determined to be the best by the programme. The calculated tree was visualized and edited using iTOL (v.6)[51].

Macrophage culture

BALB/c BMDMs were obtained as previously described[52]. Briefly, bone marrow cells were cultured for 7–9 days in RPMI 20/30, which consists of RPMI-1640 medium (Gibco, Thermo Fisher) supplemented with 20% (v/v) fetal bovine serum (FBS) and 30% (v/v) L-cell conditioned media as a source of macrophage colony-stimulating factor on non-treated Petri dishes (Optilux - Costar, Corning). At 24 h before experiments, BMDM monolayers were detached using cold PBS (Hyclone, GE Healthcare) and cultured, as specified, in RPMI-1640 (Gibco, Thermo Fisher) supplemented with 10 % (v/v) FBS, 10 U ml^{-1} penicillin and 10 mg ml^{-1} streptomycin, 2 mM L-glutamine and 25 mM HEPES, pH 7.2 (Gibco, Thermo Fisher) at 37 °C in 5% (v/v) CO_2 for the indicated periods.

Co-culture of conidia with murine alveolar macrophages (MAMs)

Primary MAMs were collected from mouse lungs with ice-cold Ca^{2+}- and Mg^{2+}-free PBS through an 18-gauge plastic catheter inserted into the trachea after cervical dissection as described previously[53]. Primary MAMs were separated from the lavage fluid by centrifugation (400 × *g* for 8 min at 4 °C), and the cell pellet was suspended in Dulbecco's modified Eagle medium (DMEM) complete medium containing 10% foetal calf serum and plated at a density of 2×10^5 cells per well in 96 ELISA plates. Non-adherent cells were removed by washing after a 2 h incubation at 37 °C in an atmosphere of 5% CO_2. The viability of the MAM preparations was >99% as judged by trypan blue dye exclusion. Cells were challenged with 10 conidia per macrophage and subsequently incubated at 4 °C for 30 min. Unbound conidia were removed by washing with cold complete DMEM medium and incubated for 24 h at 37 °C in an atmosphere of 5% (v/v) CO_2.

Macrophage infection, cytokine and LDH determination

BMDMs were cultured as previously described and seeded at a density of 1×10^6 cells per ml in 24-well plates (Greiner Bio-One). The cells were challenged with conidia of different strains at a multiplicity of infection (MOI) of 1:10 and incubated a 37 °C with 5% (v/v) CO_2 for 24 h. BMDMs were also stimulated with different concentrations of AspA protein (denaturated or not) by boilling for 10 min at 100 °C. Lipopolysaccharides (standard LPS, *E. coli* 0111: B4; Sigma-Aldrich, 500 ng ml^{-1}) plus Nigericin (tlrl-nig, InvivoGen 5 μM ml^{-1}) and medium alone were respectively used as positive and negative controls. Cell culture supernatants were collected and stored at −80 °C until they were assayed for TNF-α, IL-1 and LDH release using Mouse DuoSet ELISA kits (R&D Systems) and CyQUANT LDH cytotoxicity assay (Invitrogen), according to manufacturer instructions. For cytokine determination, plates were analysed using a microplate reader (Synergy

HTX Multi-Mode, BioTek) measuring absorbance at 450 nm. Cytokine concentrations were interpolated from a standard curve and statistical significance was determined using analysis of variance (ANOVA) (GraphPad Prism 8.0). The level of LDH was determined by measuring absorbance at 490 and 680 nm using a microplate reader (Synergy HTX Multi-Mode, BioTek). All assays were performed in triplicate in three independent experiments.

Aspergillus growth and fluorescein isothiocyanate (FITC) label

Aspergillus strains were cultivated on MM agar plates at 37 °C for 3 days. Conidia were collected in sterile water with 0.05% (v/v) Tween20.The resulting suspension was filtered through two layers of gauze (Miracloth, Calbiochem). FITC labelling of conidia was performed with 0.1 mg ml^{-1} FITC (Sigma) in 0.1 M Na_2CO_3 at 37 °C for 30 min. Labelled conidia were washed three times with PBS and 0.1% (v/v) Tween20. Conidia concentration was determined using a haemocytometer.

Phagocytosis and adhesion assays

BMDMs were cultivated in DMEM supplemented with 10% (v/v) heat-inactivated fetal calf serum, 2 mM glutamine and penicillin-streptomycin. For infection experiments, macrophages were seeded on glass cover slips in 24-well plates at a density of 5×10^5 cells per well and allowed to grow adherently overnight. Following washing with pre-warmed medium, FITC-labelled conidia were added at an MOI of 10. The infection experiment was synchronized for 30 min at 4 °C. Unbound conidia were removed by washing with pre-warmed medium and phagocytosis was initiated by shifting the co-incubation to 37 °C in a humidified CO_2 incubator. After 1 h, phagocytosis was stopped by washing with ice-cold PBS. Labelling of extracellular conidia was performed by incubation with PBS and 0.25 mg ml^{-1} Calcofluor white (Sigma) for 30 min at 4 °C. The cells were washed twice with PBS and fixed with 3.7% (v/v) formaldehyde/PBS for 15 min followed by two washes with PBS. Microscope photographs were taken on a Zeiss microscope. For statistical reproducibility, two biological replicates and in each case, two technical replicates were made and analysed for each strain. The phagocytic index was enumerated by counting 100 macrophages per cover slip from duplicate wells and calculated as the average number of conidia that had been phagocytosed for each macrophage.

Conidial killing assay

BMDMs were seeded at a density of 10^6 cells per ml in 24-well plates (Corning Costar) and challenged with conidia at an MOI of 1:10 and incubated at 37 °C with 5% (v/v) CO_2 for 24 h. After incubation media were removed, the cells were washed with ice-cold PBS and finally, 2 ml of sterile water was added to the wells. A P1000 tip was then used to scrape away the cell monolayer and the cell suspension was collected. This suspension was then diluted at 1:1,000 and 100 µl was plated on Sabouraud agar before the plates were incubated a 37 °C overnight and the colonies were counted. Of the inoculum, 50 µl adjusted to 10^3 ml^{-1} was also plated on Sabouraud dextrose agar to correct colony-forming unit (c.f.u.) counts. The c.f.u.s ml^{-1} for each sample were calculated and compared to the A1163 wild-type strain.

Acidification of phagolysosomes

Acidification of phagolysosomes was essentially determined as previously described[18]. In brief, RAW 264.7 murine macrophages were incubated in DMEM with 27.5 mg ml^{-1} gentamicin sulfate (Gibco), 10% (v/v) FBS (GE Healthcare Life Sciences) and 1% (w/v) ultraglutamine (Gibco) at 37 °C and 5% (v/v) CO_2 in a humidified incubator. Cells were pre-stained with 50 nM LysoTracker red DND-99 (Invitrogen) for 1 h before infection. Conidia were stained with 0.1 mg ml^{-1} CFW (Sigma-Aldrich) for 10–15 min before infection. Cells (1×10^5 per well) were added to 8-well ibidi slides (ibidi) and infected at an MOI of 3 with CFW-stained conidia for 2 h at 37 °C and 5% (v/v) CO_2 in a humidified incubator. Uptake of conidia was synchronized by centrifugation at 100 × *g* for 5 min. After infection, cells were washed with PBS and fixed using 3.7% (v/v) formaldehyde in PBS for 10 min, followed by a washing step with PBS. Slides were directly imaged using a Zeiss LSM 780 microscope and analysed using Zeiss ZEN software. At least 100 conidia were counted for each biological replicate. Clear red signals surrounding conidia within phagosomes were evaluated as acidified conidia. Three independent experiments were performed.

BMDMs antifungal activity

BMDMs were isolated as previously described and 5×10^5 cells were seeded in 96 round-bottom wells in complete DMEM (Gibco), 10% (v/v) FBS (Gibco), 1% (v/v) penicillin/streptomycin (Sigma) and 1% (v/v) HEPES (Gibco). After adhesion, the BMDMs were infected with 5×10^6 conidia (MOI 1:10). Upon 24 h of co-incubation, the cells were lysed with sterile water and conidia were stained for 5 min with 50 µl of a filter-sterilized 1 mg ml^{-1} Calcofluor white solution (Sigma-Aldrich). Conidia were washed with sterile water and the staining was quantified using a fluorometer at 360 nm excitation and 440 nm emission.

XTT (2,3-bis-(2-methoxy-4-nitro-5-sulfophenyl)-2*H*-tetrazoli um-5-carboxanilid) assay was performed as described[54,55]. Briefly, 5×10^5 BMDMs were plated in 96-well plates and then infected with 5×10^6 spores in a final volume of 100 µl DMEM. Control wells contained spores but no BMDMs or only BMDMs. Following a 2 h incubation, the macrophages were subjected to hypotonic lysis by three gentle washes with distilled water, followed by a 30 min incubation with distilled water at 37 °C. Supernatants were then removed, with great care taken so as not to remove the spores. DMEM without phenol red, containing 400 µg ml^{-1} of XTT and 50 µg ml^{-1} of coenzyme Q, were added and the wells incubated for 2 h at 37 °C. The optical density at 450 nm (OD_{450}) and the OD_{650} were then measured, and data were expressed as the percentage of antifungal activity according to published formula[54].

Cytokine and chemokine quantification

For lung homogenates, the lungs of all experimental groups were homogenized in PBS supplemented with Complete Mini protease inhibitor tablets (Roche), clarified by centrifugation and stored at −80 °C. A panel of cytokines and chemokines were quantified by ELISA (R&D Systems) according to manufacturer instructions.

Detection of ROS

In 96-well tissue culture-treated dark clear-bottom plates (Sigma-Aldrich), 5×10^5 BMDMs per 100 µl were infected with 5×10^6 conidia followed by 4, 8 and 24 h of incubation at 37 °C. The cells were treated with the ROS detection dye CellROX Reagent (Thermo Fisher) at a final concentration of 5 µM for 30 min at 37 °C. ROS detection was performed using a fluorescence plate reader (Thermo Fisher) at an excitation of 485 nm and an emission of 520 nm. BMDMs stimulated with 50 nM phorbol 12-myristate 13-acetate (PMA) (Sigma-Aldrich) for 20 min at 37 °C were used as positive control.

Transwell assay

BMDMs were seeded at a density of 10^6 cells per ml in 24-well plates (Corning Costar) and the assay was performed with the addition in each well of a Transwell insert (0.2 µm filter; Corning) containing medium alone, Δ*aspA-1*, Δ*aspA-2* or wild-type conidia at an MOI of 1:10 and incubated at 37 °C with 5% (v/v) CO_2 for 24 h. After incubation, cell culture supernatants were collected and stored at −80 °C until they were assayed for TNF-α and IL-1 production. In the Transwell system, the small and soluble compounds are able to migrate between the upper Transwell and the lower chamber, whereas spores are prevented from moving between the chambers.

Epithelial cell invasion assay

The capacity of the various strains to invade the A549 cells was determined using previously described methods with some modification[56,57]. The *A. fumigatus* wild-type and mutant strains were grown on Sabouraud dextrose agar (Difco) at 37 °C for 7 days before use. Conidia were collected with PBS containing 0.1% (v/v) Tween 80 (Sigma-Aldrich) and counted with a haemacytometer. The A549 pulmonary epithelial cell line (American Type Culture Collection (ATCC)) was cultured in F12 medium (ATCC) containing 10% (v/v) FBS (Gemini Bio-Products), and 2 mM L-glutamine with penicillin and streptomycin (Irvine Scientific) in 5% CO_2 at 37 °C. Before the assay, 2×10^5 A549 cells were cultured in 24-well tissue culture plates containing fibronectin-coated circular glass coverslips in each well for overnight. *A. fumigatus* conidia were pre-germinated in Sabouraud dextrose broth (Difco) at 37 °C for 5.5 h, counted and suspended in F-12K medium. Next, 1×10^5 germlings of each strain in 1 ml F-12K medium were added to A549 cells that had been grown to confluency on the glass coverslips. After incubation for 3 h, the cells were rinsed with 1 ml Hanks' balanced salt solution (HBSS) in a standardized manner and then fixed with 4% (v/v) paraformaldehyde. The non-internalized portions of the organisms were stained with polyclonal rabbit anti-*A. fumigatus* primary antibody (Meridian Life Science), followed by AlexaFluor 568-labelled secondary antibody (Life Technologies). After the coverslips were mounted inverted on microscope slides, they were viewed by epifluorescence. The number of cell-associated organisms was determined by counting the number of red fluoresced organisms per high-powered field (HPF). The number of endocytosed organisms was determined by subtracting the number of non-internalized organisms (staining of entire germlings) from the number of cell-associated organisms. At least 100 organisms per coverslip were scored and each strain was tested in triplicate.

Epithelial cell damage assay

To evaluate the capacity of various strains to damage A549 epithelial cells, we used our standard ^{51}Cr release assay[57–59]. *A. fumigatus* conidia and A549 cells were prepared as previously described. The A549 cells were grown to confluency in a 24-well tissue culture plate and then loaded with ^{51}Cr overnight. The following day, the cells were rinsed twice with HBSS to remove the unincorporated ^{51}Cr and 5×10^5 conidia of each strain in 1 ml of F-12K medium were added to triplicate wells. After 16 h of incubation, 500 μl of medium above the cells were collected and transferred to glass test tube A. Next, the remaining medium in the wells was collected and placed in glass test tube B. After lysing the A549 cells with 6 N NaOH, the lysate was collected and the wells were rinsed twice with RadiacWash (Biodex Medical Systems). The lysate and rinses were added to test tube B. The amount of ^{51}Cr in the medium and the cell lysate was measured using a gamma counter. The spontaneous release of ^{51}Cr was determined using uninfected A549 cells that were processed in parallel. The specific release of ^{51}Cr was calculated using our previously described formula. Each experiment was performed in triplicate. Mutants that caused less damage to A549 cells than the control strain were tested at least one more time to verify the results.

Animal survival curves and fungal burden

Inbred female mice (BALB/c or C57BL/6 strains; body weight 20–22 g; age 6–8 weeks) were housed in vented cages containing 5 animals. Cages were well ventilated, softly lit and subjected to a 12 h:12 h light/ dark cycle. Relative humidity was kept at 40–60%. Mouse rooms and cages were kept at a temperature of ~22 °C. Mice were immunosuppressed with cyclophosphamide (150 mg kg^{-1} body weight), which was administered intraperitoneally on days −4, −1 and 2 pre and post infection (infection day is ‘day 0’). Hydrocortisonacetate (200 mg kg^{-1} body weight) was injected subcutaneously on day −3. Mice (10 per group, two repetitions) were anaesthetized by halothane inhalation and infected by intranasal instillation of 20 μl containing 1.0×10^5 conidia of *A. fumigatus* wild-type or mutant strains, Ale, Aoe or Afi (the viability of the administered inoculum was determined by incubating different serial dilutions of the conidia used in both repetitions on MM medium at 37 °C). As a negative control, a group of 10 mice received PBS only. Animals were killed at 15 days post infection or if moribund. To investigate fungal burden in murine lungs, mice (10 per group, two repetitions) were immunosuppressed as described previously or not, and then intranasally inoculated with 1×10^6 conidia per 20 μl of suspension for the chemotherapeutic murine model and with 5×10^8 conidia per 20 μl for the immunocompetent murine model. Animals were killed at 48 h post infection, and the lungs were collected and immediately frozen in liquid nitrogen. DNA was extracted via the phenol/ chloroform method and 400 mg of total DNA from each sample were used for quantitative PCRs using primers to amplify the 18S ribosomal RNA region of *A. fumigatus* and an intronic region of mouse GAPDH (glyceraldehyde-3-phosphate dehydrogenase). Six-point standard curves were calculated using serial dilutions of genomic DNA from *A. fumigatus* and the uninfected mouse lung. Fungal and mouse DNA quantities were obtained from the threshold cycle (CT) values from the appropriate standard curves. Quantitative PCR analysis was performed using the SYBR green PCR master mix kit (Applied Biosystems) in the ABI 7500 Fast Real-Time PCR system (Applied Biosystems).

The principles that guide our studies are based on the Declaration of Animal Rights ratified by UNESCO on 27 January 1978 in its 8th and 14th articles. All protocols adopted in this study were approved by the local ethics committee for animal experiments of the University of São Paulo, Campus of Ribeirão Preto (Permit Number: 23.1.547.60.8; Characterization of virulence and immunopathogenicity of *Aspergillus* spp. in the murine model). Groups of 5 animals were housed in individually ventilated cages and cared for in strict accordance with the principles outlined by the Brazilian College of Animal Experimentation (COBEA) and the Guiding Principles for Research Involving Animals and Human Beings, American Physiological Society. All efforts were made to minimize suffering. Animals were clinically monitored at least twice daily and humanely killed if moribund (defined by lethargy, dyspnoea, hypothermia and weight loss). All stressed animals were killed by cervical dislocation.

Alveolar and interstitial neutrophil isolation and characterization

Inbred BALB/c female mice were anaesthetized by halothane inhalation and infected by intranasal instillation of 20 μl containing 5×10^8 conidia of *A. fumigatus* wild-type or Δ*aspA-1* strains. Animals were killed at 16 h post infection. Following euthanasia, mice were tracheotomized and a blunt 18-gauge needle was inserted into the trachea. Lungs were then lavaged with 1 ml PBS, and the resulting bronchoalveolar lavage fluid was centrifuged at 100 × *g* for 10 min. The supernatant was collected for cytokine analyses and the resulting cell pellets recovered after centrifugation were kept on ice until staining as described below. Lungs were minced with scalpel blades and digested with 300 μg ml^{-1} Liberase TL (Roche) and 5 U ml^{-1} DNase I in cold DMEM, mixed by pipetting and incubated at 37 °C in an incubator for 25 min. Samples were dispersed through an 18G needle and strained through a 70 μm cell strainer. Erythrocytes were lysed by incubating the samples with ACK buffer. The alveolar and interstitial neutrophil samples were washed in PBS + 2% (v/v) FBS (staining buffer), and incubated with unlabelled anti-CD16/32 antibodies (FcBlock, BD Pharmingen) to block the Fc receptors. Cells were stained with 0.1% (v/v) viability Live/Dead dye (Thermo Fisher) and subsequently stained with the following fluorescently labelled antibodies: CD45-PE-Cy7, CD11b-BV510, Ly6G-FITC and Ly6G/Ly6C-PerCP-Cy 5.5. Cells were washed with staining buffer and fixed with 2% (w/v) paraformaldehyde in PBS. The samples were acquired on an LSR Fortessa flow cytometer using FACSDiva software (BD Biosciences). Following acquisition, data were analysed using FlowJo software v.10 (FlowJo), with neutrophils being defined as $CD45^+Ly6G/Ly6C^+$ $CD11b^+$ positive cells. For gating strategy, see Extended Data Fig. 7.

Phenotypic assay

Plates containing solid MM medium were inoculated with 1×10^4 spores per strain and left to grow for 72 h at 37 or 44 °C. When required, MM was supplemented with Congo red (10 μg ml^{-1}) or H_2O_2 (1.5 mM). All radial growths were expressed as ratios, dividing colony radial diameter of growth in the stress condition by colony radial diameter in the control (MM at 37 °C) condition.

Germination assay

The germination process for the A1163 strain was followed over a 16 h time period under a Nikon TI microscope equipped with a 37 °C incubator and a ×40 objective, with 1 picture captured every 30 min using NIS-Elements 4.0 (Nikon) software. The Cell Counter plug-in of the ImageJ platform (http://rsb.info.nih.gov/ij/index.html) was employed to differentially count resting or swollen conidia versus germinated conidia. A timepoint was selected (7 h) in which A1163 achieved 50–60% germination and the knockout mutant strains were assayed for the same time point, including A1163 as a control. Conidia (10^4) were inoculated into 200 µl of liquid MM in 96-well plates and each strain was tested in technical duplicates.

Staining and labelling of cell surface components

Cell wall surface polysaccharide staining was performed as described previously[60]. Briefly, 10^4 spores for each deletion mutant and A1163 strains were inoculated in 200 µl of liquid MM and incubated for 4 h at 37 °C (swollen conidia) and 4 °C (resting conidia) before the culture medium was removed and conidia were UV irradiated (600,000 mJ). For dectin labelling, 200 µl of a blocking solution (2% (v/v) goat serum, 1% (v/v) bovine serum albumin, 0.1% (v/v) Triton X-100, 0.05% (v/v) Tween 20, 0.05 % (v/v) sodium azide and 0.01 M PBS) was added to each well. Samples were incubated for 30 min at room temperature (r.t.) and 0.2 µg ml^{-1} of Fc-h-dectin-hFc (Invivogen) was added to the UV-irradiated conidia and incubated for 1 h at r.t., followed by the addition of 1:1,000 DyLight 594-conjugated goat anti-human IgG1 (Abcam) for 1 h at r.t. Conidia were then washed with PBS, and fluorescence was read at 587 nm excitation and 615 nm emission. For chitin staining, 200 µl of a PBS solution with 10 mg ml^{-1} of CFW was added to the UV-irradiated conidia, which were incubated for 5 min at r.t. and washed with PBS before fluorescence was read at 380 nm excitation and 450 nm emission. For *N*-acetyl-D-glucosamine (GlcNAc) labelling, 200 µl of PBS supplemented with 0.1 mg ml^{-1} of WGA lectin (lectin-FITC L4895; Sigma) was added to the UV-irradiated germlings for 1 h at r.t. Germlings were washed with PBS, and fluorescence was read at 492 nm excitation and 517 nm emission. All experiments were performed using at least 4 repetitions, and fluorescence was read in a microtitre plate reader (Synergy HTX Multimode Reader, Agilent Biotek or EnSpire Multimode Plate Reader, Perkin Elmer).

Fungal adhesion assay

To determine the adhesion capacity of conidia from deletion mutant and A1160 strains, 1×10^4 conidia were inoculated into 200 µl liquid MM in a 96-well polystyrene microtitre plate. Following an initial adherence phase of 4 h during static incubation at 37 °C (swollen conidia) or 4 °C (resting conidia), unbound conidia were washed with sterile PBS. Fresh liquid MM was added to the adhered conidia, and static submerged cultures were grown for up to 24 h at 37 °C. Subsequently, the plate was washed exhaustively with PBS before incubation with 200 µl 0.5% (w/v) crystal violet solution for 5 min at r.t. The stained mycelia were then exhaustively washed with sterile water and air dried. Finally, the crystal violet was eluted from the wells using 100% ethanol, and absorbance was measured at 590 nm in a Synergy HTX Multimode Reader (Agilent Biotek).

To check conidial adhesion to immortalized lung cells, a total of 1×10^5 A549 cells were plated in DMEM medium in each well of a 6-well plate culture and allowed to grow to confluence at 37 °C under 5% (v/v) CO_2. Then, the wells were overlaid with fresh DMEM medium containing 100 conidia per well and incubated for 2 h at 37 °C under 5% (v/v) CO_2. The wells were then rinsed three times with pre-warmed PBS, overlaid with Sabouraud's dextrose aga, and incubated at 37 °C for 36 h. Fungal colonies derived from the conidia that adhered to the cells (or to the wells) were counted. Conidial adherence levels were calculated by dividing the number of adherent conidia by the number of conidia added to the well and expressing the resulting value as a percentage. All experiments were performed in triplicate.

Assessment of conidial hydrophobic properties

The distribution of conidia on a water–oil interface was determined by the addition of 1×10^8 conidia of the wild-type and each deletion strain in a solution containing water and tributyrin (1:1 (v/v)). The mixture was vortexed for 1 min and allowed to stand for 1 h to allow the conidia to disperse. The distribution of the conidia for each mutant were then visually compared to that of the A1163 wild-type strain.

L-asparaginase activity

The L-asparaginase activity was determined according to the method described in ref. 61 with modifications. The reaction mixture consisted of 5 µl of 0.1 M L-asparagine solution, 10 µl of Tris-HCl buffer (0.05 M, pH 8.6) and 5 µl of an enzyme, making up the total volume to 20 µl. The microplates were incubated at 37 °C for 30 min. The reaction was halted by adding 5 µl of 1.5 M trichloroacetic acid. The control was prepared with buffer. These reactions (20 µl) were assessed colorimetrically by adding 160 µl of water and 20 µl of Nessler's reagent, and absorbance was measured using a microplate spectrophotometer (Spectra Max Plus 384, Molecular Devices) at 436 nm. The amount of released ammonia was calculated using an ammonium (ammonium sulfate) standard curve. One unit (U) of L-asparaginase was defined as the amount of enzyme catalysing the formation of 1 µM of ammonia from L-asparagine per minute at 37 °C and pH 8.6.

Statistical analysis

Statistical significance for each experiment was established using two-sided one-way or two-way ANOVA using the built-in tools of Prism 6. Statistical tests and *P* values are indicated in the figure legends and were chosen on the basis of the nature of the experiment and standard tests employed in the field. Underlying assumptions for these tests, including sample independence, variance equality and normality were assumed to be met. ANOVA was followed by Tukey's, Dunnett's or Bonferroni's multiple comparisons test when appropriate. Multivariate analyses of the phenotypes were done using principal component analysis with the prcomp programme in R with scaled variables, and the correlation among the variables using the Pearson method (stats package v.3.5.2). The plots were generated using the ggplot2 (v.3.4.4) package[62]. To compare the dispersions between *A. fumigatus* and Afi phenotypes, Levene's test was applied using the R package car (v.3.1–2)[63,64].

Reporting summary

Further information on research design is available in the Nature Portfolio Reporting Summary linked to this article.

Extended Data

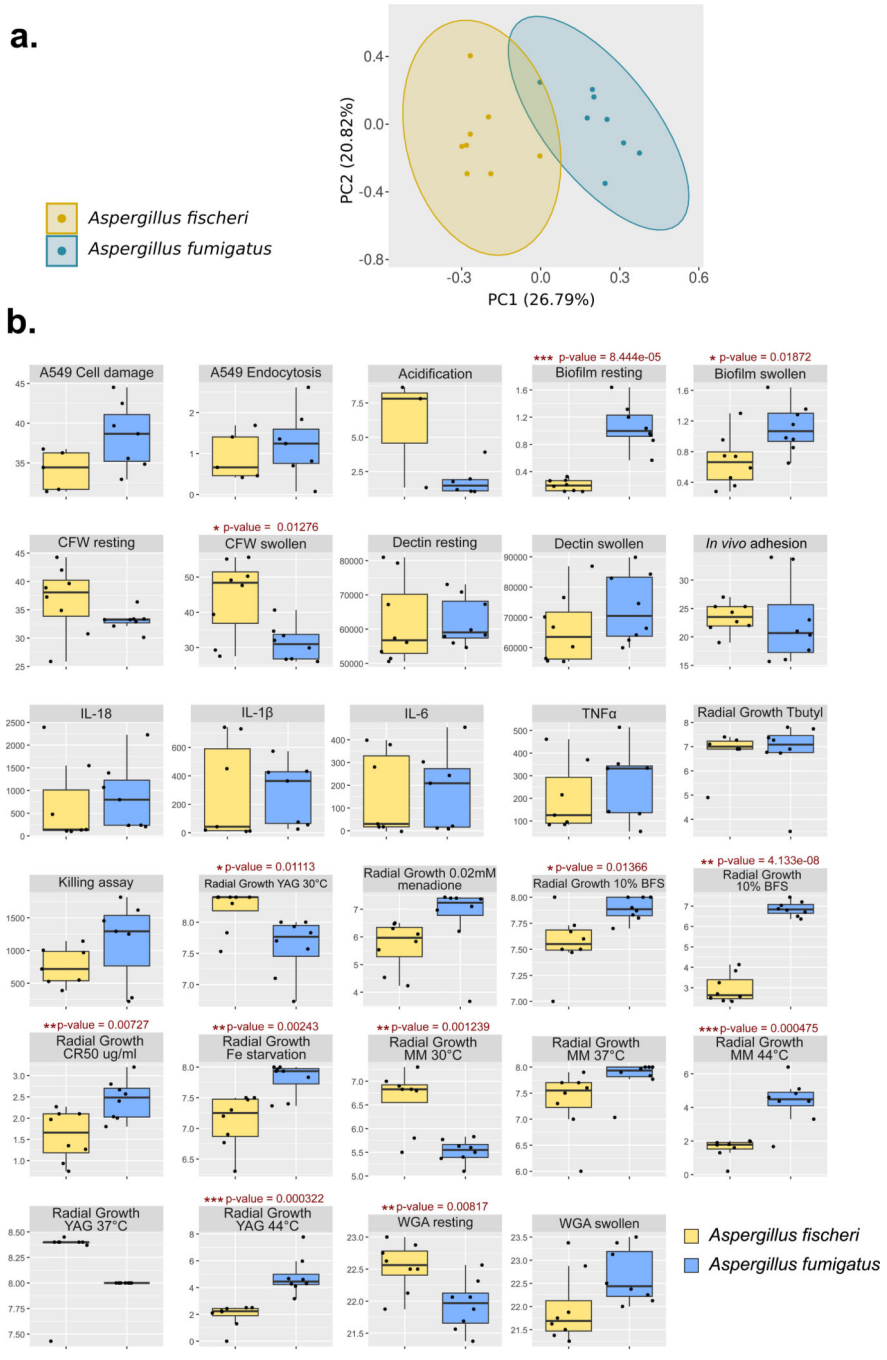

Extended data Fig. 1 |. Phenotypic comparison between *A. fumigatus* and *A. fischeri* isolates (n=8).

Statistical Multivariate analyses of fungal phenotypes. **a**. Principal component analysis (PCA) based on the measure of different phenotypes. **b**. Boxplots comparing twelve statistically different phenotypes and nine non statistically different phenotypes of *A. fumigatus* and *A. fischeri*. Statistical differences are shown for two-sided Welch t-test (p-values: *, <0.05; **, <0.01; and ***, <0.001). The median and the first and third quartiles of the distribution are represented in the box, with whiskers extending ±1.5 × interquartile range, considering points outside as outliers.

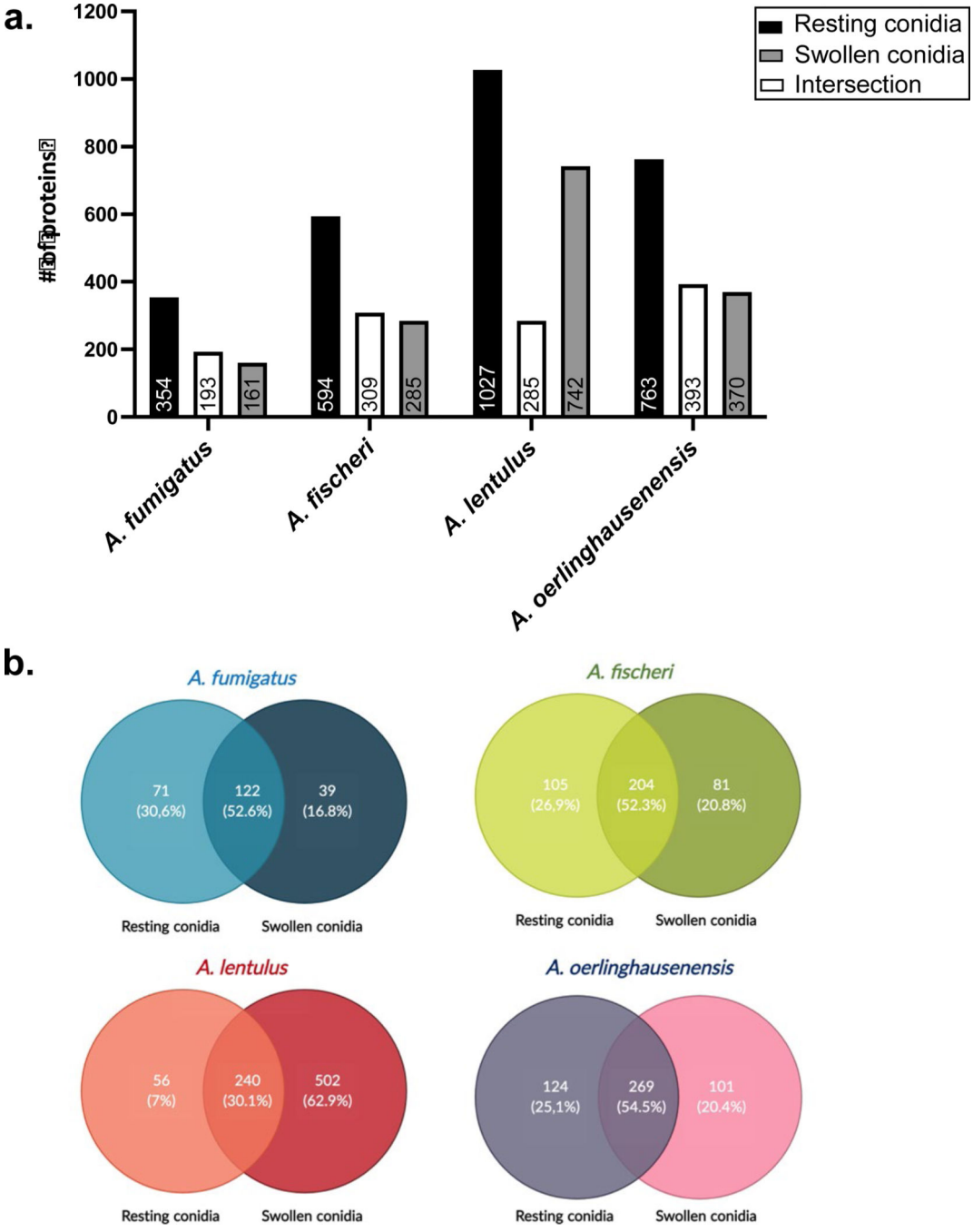

Extended data Fig. 2 |. Proteins identified by trypsin-shaving in resting and swolllen conidia of the four *Aspergillus* species included in this work.

a. Number (#) of proteins (n=3 biological repetitions). The # of proteins represent the selected results of the product of the total number of identified peptide sequences (peptide spectrum matches) for a specific protein divided by the number of aminoacids multiplied by the coverage (the percent coverage calculated by dividing the number of amino acids in all found peptides by the total number of amino acids in the entire protein sequence, and divided by 100) (PSMs/AAs)*(Cov/100) > 0.001). **b**. Venn diagrams ilustrating the intersection of proteins identified by trypsin shaving of resting and swollen conidia of *Aspergillus* spp. strains.

Extended data Fig. 3 |. Hydrophobicity of A. fumigatus conidia.

Distribution of conidia of *A. fumigatus* wild-type A1163 and deleted mutant strains in a 1:1 water-oil (tributyrin) interface.

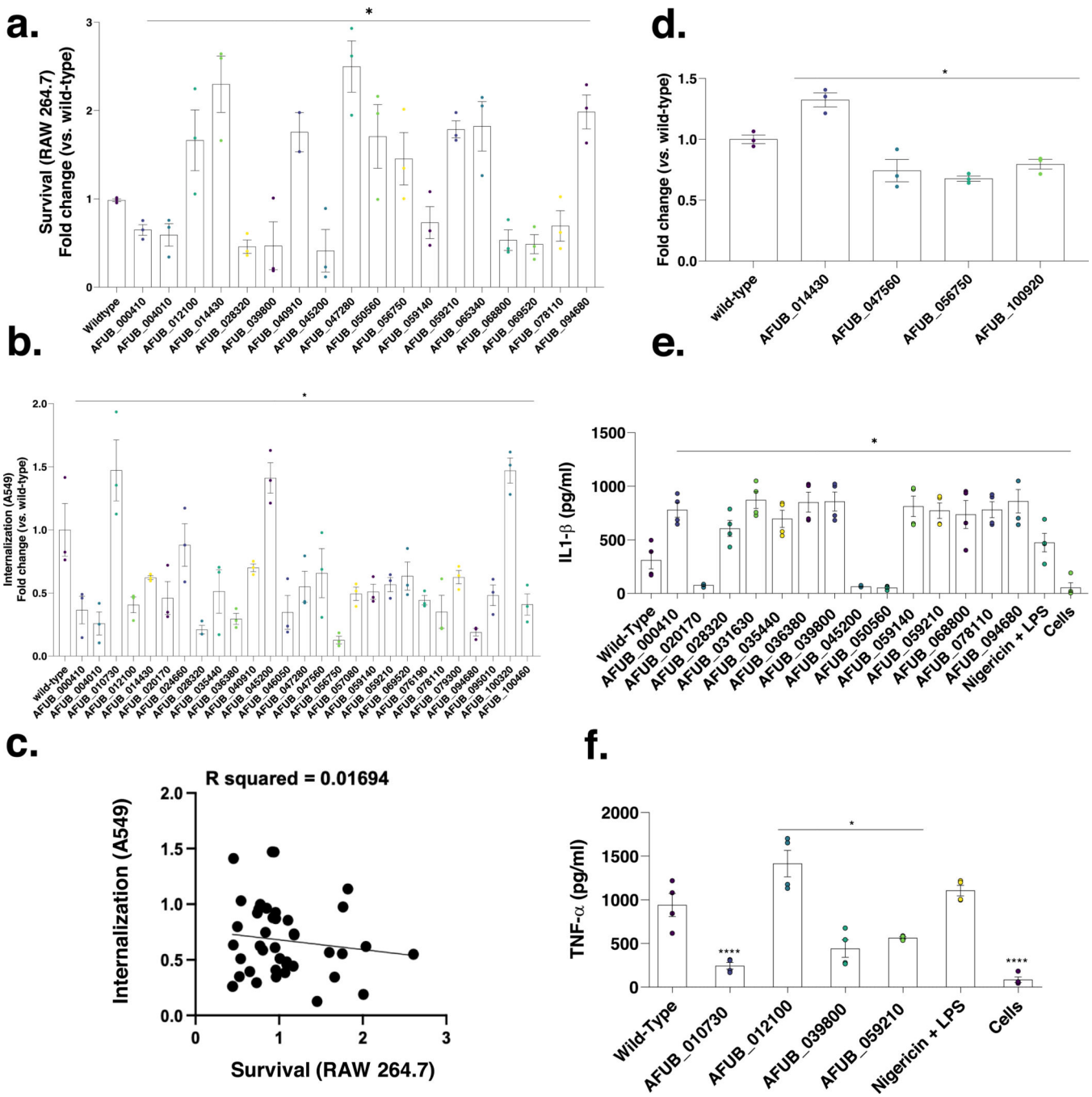

Extended data Fig. 4 |. *A. fumigatus* surface-associated proteins are involved in host-pathogen interactions.

a. Conidia survival of deleted mutants in murine RAW 264.7 macrophages at 6 hpi expressed as fold change against A1163 wild-type strain. **b**. Conidia internalization in A549 epithelial cells at 3 hpi expressed as fold change against A1163 (wild-type) strain. **c**. Simple linear regression models of **a**. and **b**. datasets (no correlation). Thresholds of 30 %-fold change above (red) and below (green) the wild-type strain (A1163) condition were established for statistical significance testing. **d**. Damage to A549 epithelial cells as

measured by specific ^{51}Cr release. **e** and **f**. *A. fumigatus* wild-type and mutant conidia eliciting cytokines IL-1β and TNF-α production by BMDMs. The results are given as the average of three independent biological repetitions and are expressed as average ± standard deviation. Statistical analysis was performed using two-sided One-way ANOVA with Dunnettś multiple comparisons test for comparisons to the wild-type strain (A1163) (*p < 0.05).

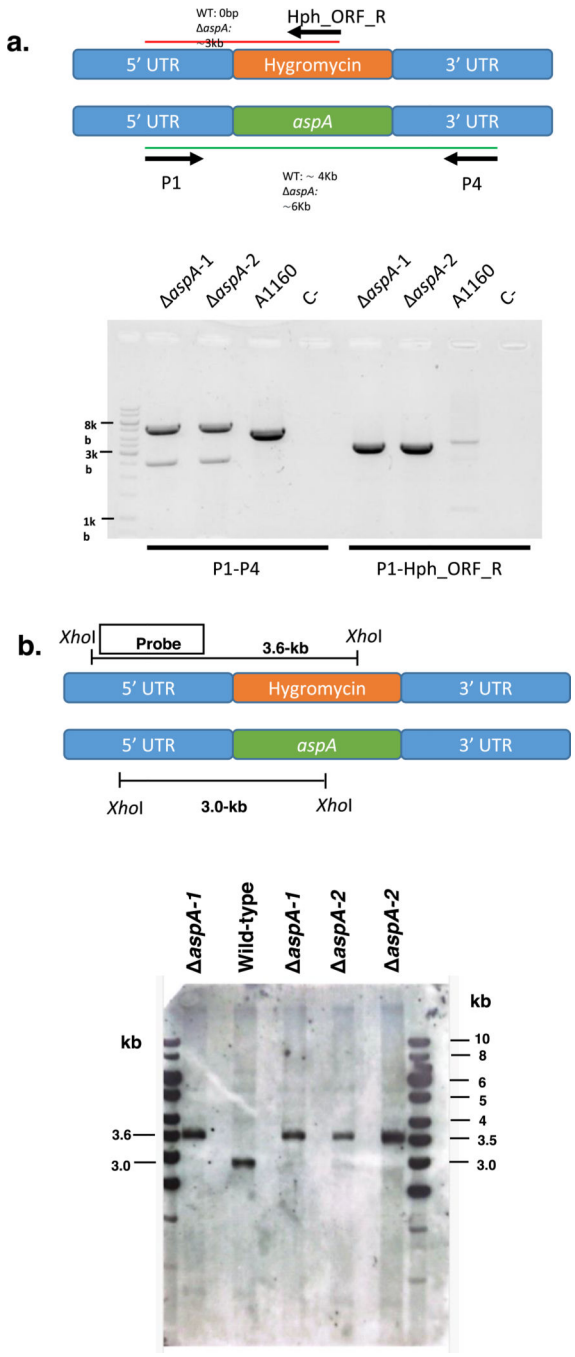

Extended data Fig. 5 |. Validation of A. fumigatus mutants.

a. Diagnostic PCR and b. Southern blot for *Aspergillus fumigatus* Δ*aspA* mutants. Both PCR and Southern blot experiments were repeated twice and those figures are representative images of the experiments.

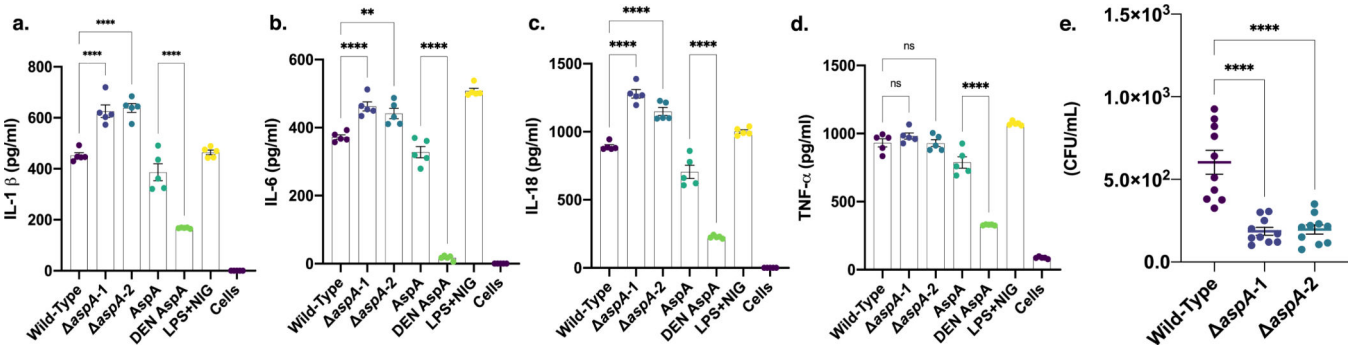

Extended data Fig. 6 |. *A. fumigatus* Δ*aspA* mutant has reduced viability in the presence of alveolar macrophages and can modulate IL-1β, IL-6, IL-18, but not TNF-α.

a to **d**. Δ*aspA* conidia modulate cytokine production upon exposure of the wild-type and Δ*aspA* mutants to alveolar macrophages for 24 h. **e**. Δ*aspA* mutants have reduced viability by the BMDMs when compared to the wild-type strain. **a** to **d**. Heterologously expressed AspA can modulate IL-1β, IL-6, IL-18, and TNF-α levels production by alveolar macrophages. Denatured AspA has decreased cytokine production in alveolar macrophages. The statistical analysis was performed using a two-sided One-way ANOVA (Tukey's test) for multiple comparisons. The results graphic shows the value of five to ten biological replicates ± standard deviation, with adjusted (adj.) P values. **adj. 0,0015, ****adj. P < 0.0001. ns not significant.

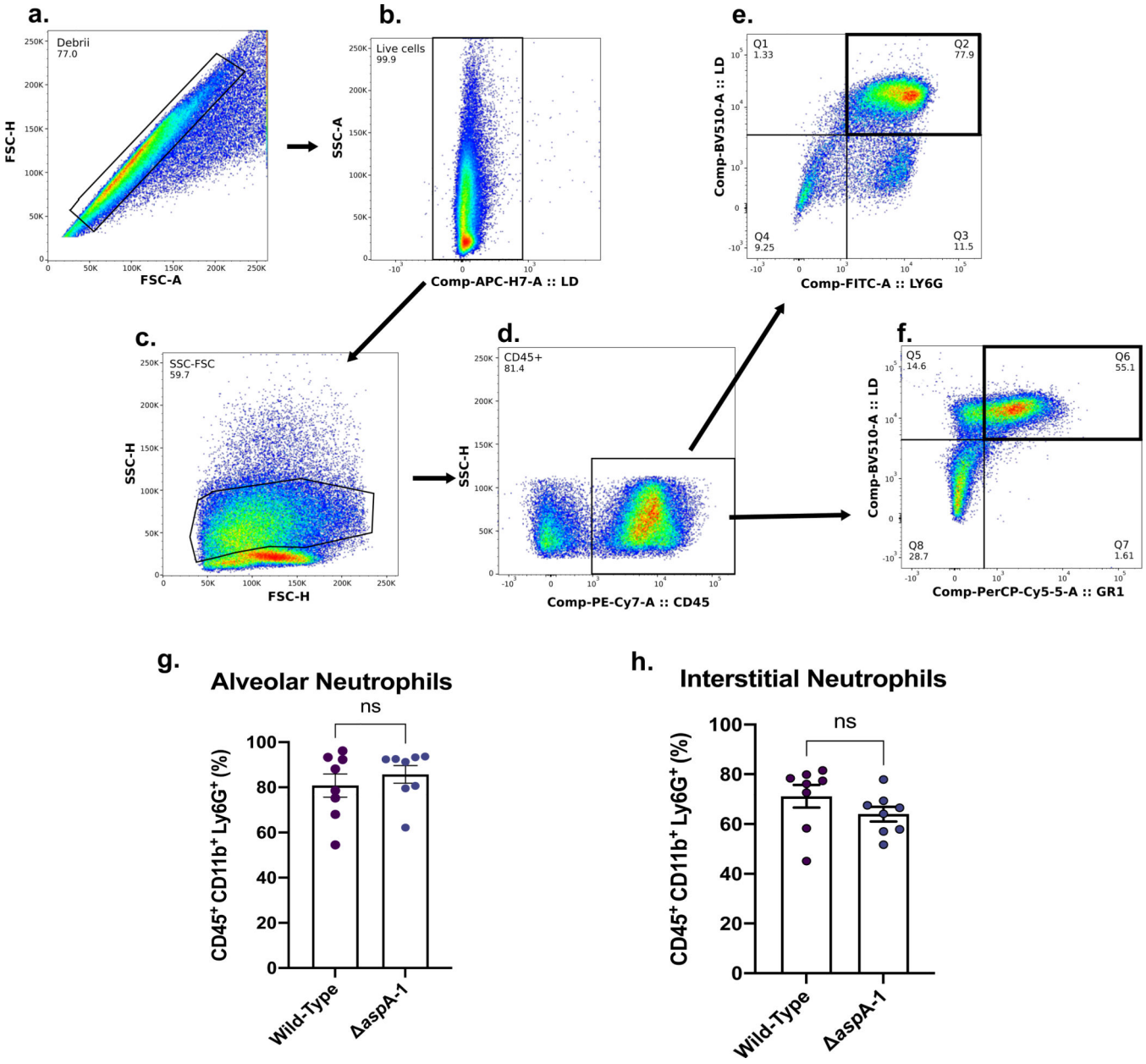

Extended data Fig. 7 |. Gating procedure used to quantify the CD45+ CD11b+ Ly6G+ and CD45+ CD11b+ Ly6G/Ly6C+ triple-positive neutrophil populations.

Arrows indicate the gate selected and carried forward for the next analysis. After gating for single cells (**a**.) and live cells (**b**. and **c**.), the resulting population was gated for CD45+ myeloid cells (**d**.), followed by gating for Ly6G+ CD11b+ (**e**.) and for Ly6G/Ly6C+ CD11b+ double-positive cells (**f**.) within the CD45+ population. The results graphic shows the percentage of CD45+ CD11b+ Ly6G+ positive cells in mice infected with 5×10^8 conidia of *A. fumigatus* wild-type or Δ*aspA-1* strains (eight biological replicates ± standard deviation) (**g**. and **h**.). The *p*-values for the comparison between the groups were calculated using non-parametric t-test (two-tailed) with Mann-Whitney correction ($p > 0.05$).

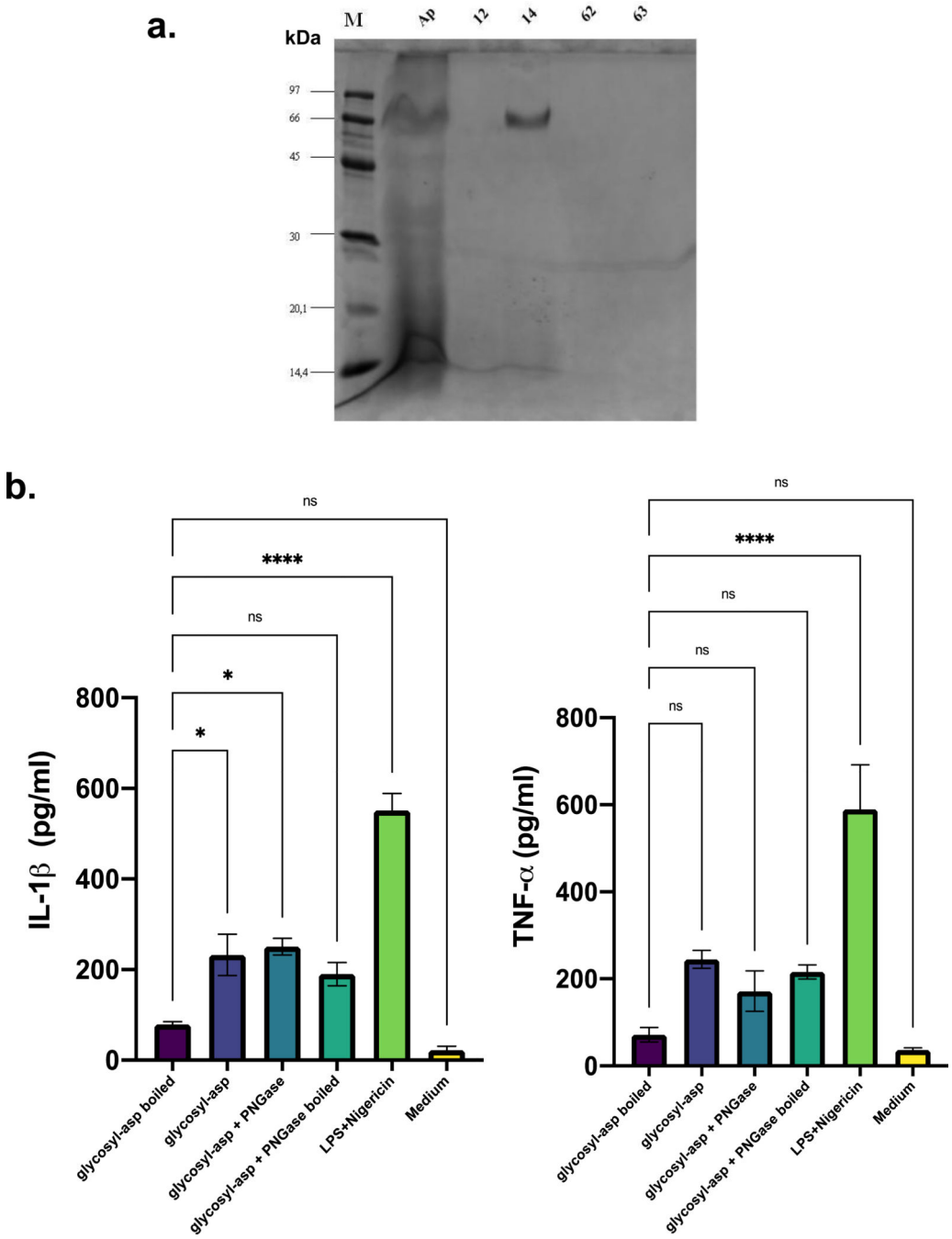

Extended data Fig. 8 |. Heterologously expressed AspA.

a. SDS polyacrilamide gel showing the purified heterologously expressed AspA in *Pichia pastoris*. Ap, raw extract; fractions 12, 14, 62, and 63. **b**. IL-1β and TNF-α production in the presence of AspA treated or not with Peptide:N-glycosidase F (PNGaseF). The statistical analysis was performed using a two-sided One-way ANOVA (Bonferroni's test) for multiple comparisons. Data are presented as values from three biological experiments ± standard deviation, *$p < 0.01$, ****$p < 0.0001$ vs glycosyl-asp boiled. ns. not significant.

Supplementary Material

Refer to Web version on PubMed Central for supplementary material.

Acknowledgements

We thank Fundação de Amparo à Pesquisa do Estado de São Paulo (FAPESP) grants numbers 2021/04977–5 (G.H.G.), 2018/18257–1 (G.P.), 2018/15549–1 (G.P.), 2020/04923–0 (G.P.), 2022/08796–8 (C.D.) and 2022/13603–4 (E.D.); Conselho Nacional de Desenvolvimento Científico e Tecnológico (CNPq) grant numbers 301058/2019–9, 404735/2018–5 and 405934/2022–0 (The National Institute of Science and Technology INCT Funvir, Fundação Coordenação de Aperfeiçoamento do Pessoal do Ensino Superior, CAPES) (Brazil, G.H.G.), and the National Institutes of Health/National Institute of Allergy and Infectious Diseases grant R01 AI153356 (USA, to A.R. and G.H.G.). This work was also funded by the Joint Canada-Israel Health Research Program, jointly supported by the Azrieli Foundation, Canada's International Development Research Centre, Canadian Institutes of Health Research, and the Israel Science Foundation (G.H.G.). This work was supported by the Deutsche Forschungsgemeinschaft (DFG, German Research Foundation) Collaborative Research Centre/Transregio FungiNet 124 'Pathogentic fungi and their human host: Networks of Interaction' (project number 210879364; projects A1 and Z2). Work was also supported by a grant from the Wellcome Trust through 'The *Aspergillus fumigatus* gene and non-coding RNA knockout library 'COFUN' (Project number 208396/Z/17/Z to M.J.B.). S.G. was co-funded by NIHR Manchester Biomedical Research Centre, the Manchester Academy of Health Sciences, the Fungal Infection Trust, the Dowager Countess Eleanor Peel trust and the Medical Research Council (MC_PC_21021). K.E. was supported by an NC3Rs studentship (NC/T001798/1). We also thank the Core Facility for Scientific Research – University of São Paulo (CEFAP-USP/BIOMASS - Mass Spectrometry and Proteome Research) for the mass spectrometry analysis. G.P. is also supported by an Honorary Associate Professorship at Macquarie University, Sydney, Australia.

Data availability

The mass spectrometry proteomics data have been deposited to the ProteomeXchange Consortium via the PRIDE partner repository[56] with the dataset identifiers PXD031199 and PXD044190. Source data are provided with this paper.

References

1. Earle K et al. Pathogenicity and virulence of *Aspergillus fumigatus*. Virulence 14, 2172264 (2023).
2. Rokas A et al. Evolving moldy murderers: *Aspergillus* section Fumigati as a model for studying the repeated evolution of fungal pathogenicity. PLoS Pathog. 16, e1008315 (2020).
3. Bayry J et al. Surface structure characterization of *Aspergillus fumigatus* conidia mutated in the melanin synthesis pathway and their human cellular immune response. Infect. Immun. 82, 3141–3153 (2014). [PubMed: 24818666]
4. Heinekamp T et al. Interference of *Aspergillus fumigatus* with the immune response. Semin. Immunopathol. 37, 141–152 (2015). [PubMed: 25404120]
5. Blango MG et al. Dynamic surface proteomes of allergenic fungal conidia. J. Proteome Res. 19, 2092–2104 (2020). [PubMed: 32233371]
6. Aimanianda V et al. Surface hydrophobin prevents immune recognition of airborne fungal spores. Nature 460, 1117–1121 (2009). [PubMed: 19713928]
7. Valsecchi I et al. Role of hydrophobins in *Aspergillus fumigatus*. J. Fungi 4, 2 (2017).
8. Voltersen V et al. Proteome analysis reveals the conidial surface protein CcpA essential for virulence of the pathogenic fungus Aspergillus fumigatus. mBio 9, e01557–18 (2018).
9. Jia LJ et al. *Aspergillus fumigatus* hijacks human p11 to redirect fungal-containing phagosomes to non-degradative pathway. Cell Host Microbe 31, 373–388 (2023). [PubMed: 36893734]
10. Asif AR et al. Proteome of conidial surface associated proteins of *Aspergillus fumigatus* reflecting potential vaccine candidates and allergens. J. Proteome Res. 5, 954–962 (2006). [PubMed: 16602703]
11. Jia LJ et al. Biotinylated surfome profiling identifies potential biomarkers for diagnosis and therapy of *Aspergillus fumigatus* infection. mSphere 5, e00535–20 (2020).

12. Suh MJ et al. Development stage-specific proteomic profiling uncovers small, lineage specific proteins most abundant in the *Aspergillus fumigatus* conidial proteome. Prot. Sci. 10, 30 (2012).
13. Venugopalan LP et al. Comparative proteome analysis identifies species-specific signature proteins in *Aspergillus* pathogens. Appl. Microbiol. Biotechnol. 107, 4025–4040 (2023). [PubMed: 37166481]
14. Yu SY et al. Clinical and microbiological characterization of invasive pulmonary aspergillosis caused by *Aspergillus lentulus* in China. Front. Microbiol. 11, 1672 (2020). [PubMed: 32849346]
15. Houbraken J, Weig M & Groβ U *Aspergillus oerlinghausenensis*, a new mould species closely related to *A. fumigatus*. FEMS Microbiol. Lett. 363, fnv236 (2016).
16. Steenwyk JL et al. Variation among biosynthetic gene clusters, secondary metabolite profiles, and cards of virulence across *Aspergillus* species. Genetics 216, 481–497 (2020). [PubMed: 32817009]
17. Mead ME et al. Characterizing the pathogenic, genomic, and chemical traits of *Aspergillus fischeri*, a close relative of the major human fungal pathogen *Aspergillus fumigatus*. mSphere 4, e00018–19 (2019).
18. Thywißen A et al. Conidial dihydroxynaphthalene melanin of the human pathogenic fungus *Aspergillus fumigatus* interferes with the host endocytosis pathway. Front. Microbiol. 2, 96 (2011). [PubMed: 21747802]
19. Horta MAC et al. Examination of genome-wide ortholog variation in clinical and environmental isolates of the fungal pathogen *Aspergillus fumigatus*. mBio 13, e0151922 (2022).
20. Baltussen TJH et al. The C_2H_2 transcription factor SltA is required for germination and hyphal development in *Aspergillus fumigatus*. mSphere 1, e0007623 (2023).
21. Zhao C et al. High-throughput gene replacement in *Aspergillus fumigatus*. Curr. Protoc. Microbiol. 54, e88 (2019). [PubMed: 31518064]
22. Mead ME et al. An evolutionary genomic approach reveals both conserved and species-specific genetic elements related to human disease in closely related *Aspergillus* fungi. Genetics 218, iyab066 (2021).
23. Latgé JP & Chamilos G *Aspergillus fumigatus* and aspergillosis in 2019. Clin. Microbiol. Rev. 33, e00140–18 (2019).
24. Shifrin S, Parrott CL & Luborsky SW Substrate binding and intersubunit interactions in L-asparaginase. J. Biol. Chem. 249, 1335–1340 (1974). [PubMed: 4594124]
25. Tarentino AL & Plummer TH Jr. Enzymatic deglycosylation of asparagine-linked glycans: purification, properties, and specificity of oligosaccharide-cleaving enzymes from *Flavobacterium meningosepticum*. Methods Enzymol. 230, 44–57 (1994). [PubMed: 8139511]
26. Steenwyk JL et al. A robust phylogenomic time tree for biotechnologically and medically important fungi in the Genera *Aspergillus* and *Penicillium*. mBio 10, e00925–19 (2019).
27. Boucher MJ & Madhani HD Convergent evolution of innate immune-modulating effectors in invasive fungal pathogens. Trends Microbiol. 32, 435–447 (2023). [PubMed: 37985333]
28. Dang EV et al. Secreted fungal virulence effector triggers allergic inflammation via TLR4. Nature 608, 161–167 (2022). [PubMed: 35896747]
29. Arvio M & Mononen I Aspartylglycosaminuria: a review. Orphanet J. Rare Dis. 11, 162 (2016). [PubMed: 27906067]
30. Mononen I et al. Aspartylglycosaminuria: protein chemistry and molecular biology of the most common lysosomal storage disorder of glycoprotein degradation. FASEB J. 7, 1247–1256 (1993). [PubMed: 8405810]
31. Mononen I & Aronson NN (eds) Lysosomal Storage Disease: Aspartylglycosaminuria (Springer, 1997).
32. Goodspeed K, Feng C, Laine M & Lund TC Aspartylglucosaminuria: clinical presentation and potential therapies. J. Child Neurol. 36, 403–414 (2021). [PubMed: 33439067]
33. Shibayama K et al. Biochemical and pathophysiological characterization of *Helicobacter pylori* asparaginase. Microbiol. Immunol. 55, 408–417 (2011). [PubMed: 21395663]
34. Washington EJ, Banfield MJ & Dangl JL What a difference a Dalton makes: bacterial virulence factors modulate eukaryotic host cell signaling systems via deamidation. Microbiol. Mol. Biol. Rev. 77, 527–539 (2013). [PubMed: 24006474]

35. Gouzy A et al. *Mycobacterium tuberculosis* exploits asparagine to assimilate nitrogen and resist acid stress during infection. PLoS Pathog. 10, e1003928 (2014).
36. McLaughlin PA et al. Contribution of asparagine catabolism to *Salmonella* virulence. Infect. Immun. 85, e00740–16 (2017).
37. Torres A et al. Asparagine deprivation mediated by *Salmonella* asparaginase causes suppression of activation-induced T cell metabolic reprogramming. J. Leukoc. Biol. 99, 387–398 (2016). [PubMed: 26497246]
38. Kelo E, Noronkoski T & Mononen I Depletion of L-asparagine supply and apoptosis of leukemia cells induced by human glycosylasparaginase. Leukemia 23, 1167–1171 (2009). [PubMed: 19158835]
39. Schmidt F et al. Flotillin-dependent membrane microdomains are required for functional phagolysosomes against fungal infections. Cell Rep. 18, 108017 (2020).
40. Amin S et al. Melanin dependent survival of *Apergillus fumigatus* conidia in lung epithelial cells. Int. J. Med. Microbiol. 304, 626–636 (2014). [PubMed: 24836942]
41. Seidel C et al. Phagolysosomal survival enables non-lytic hyphal escape and ramification through lung epithelium during *Aspergillus fumigatus* infection. Front. Microbiol. 11, 1955 (2020). [PubMed: 32973709]
42. Jahn B et al. PKSP-dependent reduction of phagolysosome fusion and intracelular kill of *Aspergillus fumigatus* conidia by human monocyte-derived macrophages. Cell. Microbiol. 4, 793–803 (2002). [PubMed: 12464010]
43. Chaveroche MK, Ghigo JM & d'Enfert C A rapid method for efficient gene replacement in the filamentous fungus *Aspergillus nidulans*. Nucleic Acids Res. 28, e97 (2000). [PubMed: 11071951]
44. Colot HH et al. A high-throughput gene knockout procedure for *Neurospora* reveals functions for multiple transcription factors. Proc. Natl Acad. Sci. USA 103, 10352–10357 (2006). [PubMed: 16801547]
45. Shah AD et al. LFQ-Analyst: an easy-to-use interactive web platform to analyze and visualize label-free proteomics data preprocessed with MaxQuant. J. Proteome Res. 19, 204–211 (2020). [PubMed: 31657565]
46. Laemmli UK Cleavage of structural proteins during the assembly of the head of bacteriophage T4. Nature 227, 680–685 (1970). [PubMed: 5432063]
47. Johnson M et al. NCBI BLAST: a better web interface. Nucleic Acids Res. 36, W5–W9 (2008). [PubMed: 18440982]
48. Sayers EW et al. Database resources of the National Center For Biotechnology Information. Nucleic Acids Res. 50, D20–D26 (2022). [PubMed: 34850941]
49. Katoh K, Rozewicki J & Yamada KD MAFFT online service: multiple sequence alignment, interactive sequence choice and visualization. Brief. Bioinform. 20, 1160–1166 (2019). [PubMed: 28968734]
50. Nguyen LT, Schmidt HA, von Haeseler A & Minh BQ IQ-TREE: a fast and effective stochastic algorithm for estimating maximum-likelihood phylogenies. Mol. Biol. Evol. 32, 268–274 (2015). [PubMed: 25371430]
51. Letunic I & Bork P Interactive Tree Of Life (iTOL) v5: an online tool for phylogenetic tree display and annotation. Nucleic Acids Res. 49, W293–W296 (2021). [PubMed: 33885785]
52. Marim FM, Silveira TN, Lima DS Jr & Zamboni DS. A method for generation of bone marrow-derived macrophages from cryopreserved mouse bone marrow cells. PLoS ONE 5, e15263 (2010).
53. Philippe B et al. Killing of *Aspergillus fumigatus* by alveolar macrophages is mediated by reactive oxidant intermediates. Infect. Immun. 71, 3034–3042 (2003). [PubMed: 12761080]
54. Ramirez-Ortiz ZG et al. A nonredundant role for plasmacytoid dendritic cells in host defense against the human fungal pathogen *Aspergillus fumigatus*. Cell Host Microbe 9, 415–424 (2011). [PubMed: 21575912]
55. Meshulam T, Levitz SM, Christin L & Diamond RD A simplified new assay for assessment of fungal cell damage with the tetrazolium dye, (2,3)-bis-(2-methoxy-4-nitro-5-sulphenyl)-(2H)-tetrazolium-5-carboxanilide (XTT). J. Infect. Dis. 172, 1153–1156 (1995). [PubMed: 7561202]
56. Liu H et al. Determining *Aspergillus fumigatus* transcription factor expression and function during invasion of the mammalian lung. PLoS Pathog. 17, e1009235 (2021).

57. Liu H et al. *Aspergillus fumigatus* CalA binds to integrin α5β1 and mediates host cell invasion. Nat. Microbiol. 2, 16211 (2016). [PubMed: 27841851]
58. Ejzykowicz DE et al. The *Aspergillus fumigatus* transcription factor Ace2 governs pigment production, conidiation and virulence. Mol. Microbiol. 72, 155–169 (2009). [PubMed: 19220748]
59. Bertuzzi M et al. The pH-responsive PacC transcription factor of *Aspergillus fumigatus* governs epithelial entry and tissue invasion during pulmonary aspergillosis. PLoS Pathog. 10, e1004413 (2014).
60. Winkelstroter LK et al. High osmolarity glycerol response PtcB phosphatase is important for *Aspergillus fumigatus* virulence. Mol. Microbiol. 96, 42–54 (2015). [PubMed: 25597841]
61. El-Naggar NA et al. Purification, characterization, cytotoxicity and anticancer activities of L-asparaginase, anti-colon cancer protein, from the newly isolated alkaliphilic *Streptomyces fradiae* NEAE-82. Sci. Rep. 6, 32926 (2016). [PubMed: 27605431]
62. Villanueva RAM & Chen ZJ ggplot2: elegant graphics for data analysis (2nd edn). Measurement 17, 160–167 (2019).
63. Fox J & Weisberg S An R Companion to Applied Regression 2nd edn Ch. 4 (Sage, 2019).
64. Perez-Riverol Y et al. The PRIDE database and related tools and resources in 2019: improving support for quantification data. Nucleic Acids Res. 47, D442–D450 (2019). [PubMed: 30395289]
65. Brown A et al. Extensive non-coding sequence divergence between the major human pathogen *Aspergillus fumigatus* and its relatives. Front. Fungal Biol. 3, 802494 (2022).

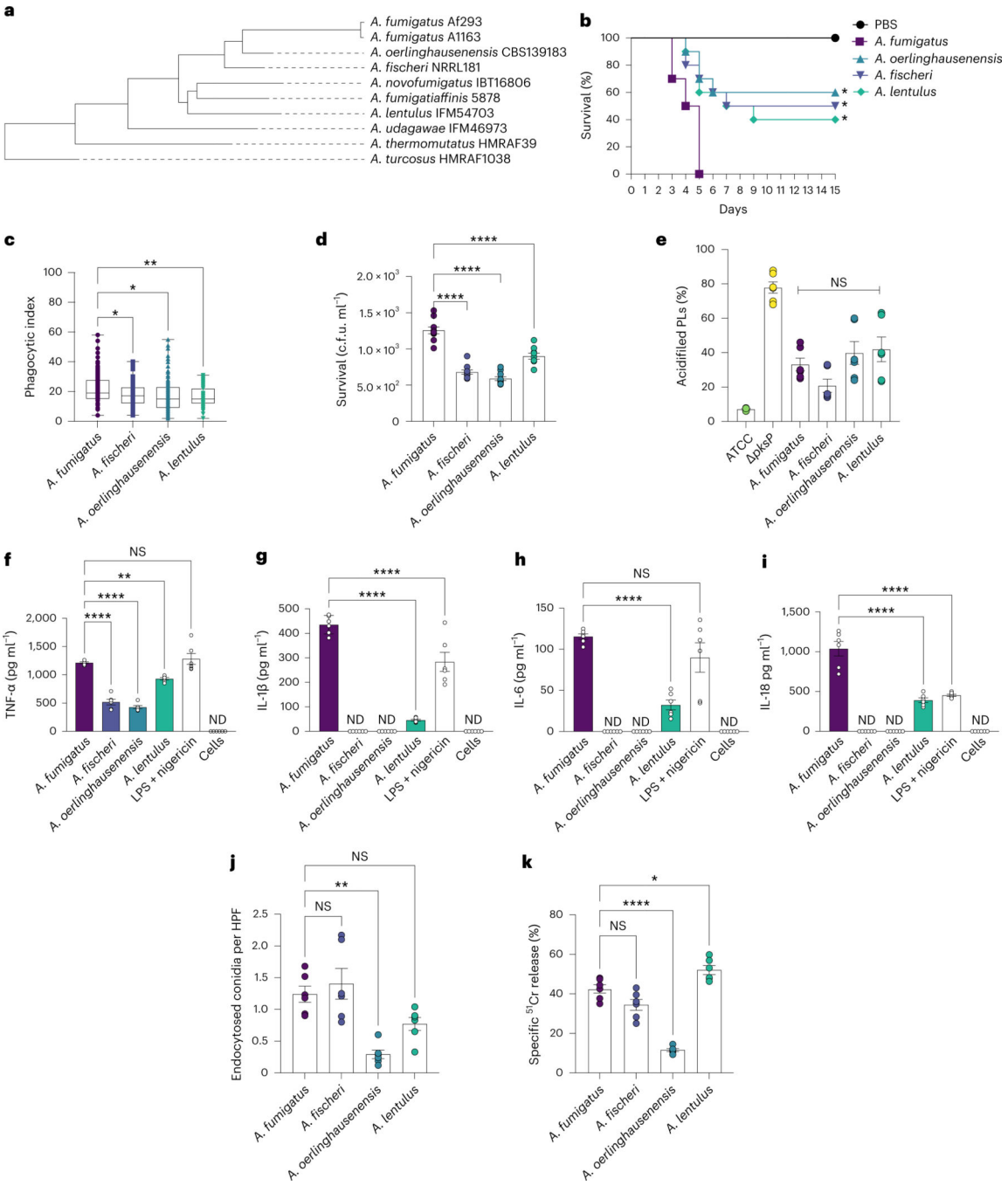

Fig. 1 |. *A. fumigatus* has increased virulence and triggers higher cytokine production by BMDMs than the other three species.

a, Phylogeny of *Aspergillus* section Fumigati representative species constructed from concatenation analysis of a 5,215-gene data matrix. Branch lengths correspond to nucleotide substitutions per site. Adapted from ref. 65. **b**, Survival curves for *A. fumigatus*, *A. fischeri*, *A. oerlinghausenensis* and *A. lentulus* in a chemotherapeutic murine model of IPA. log-rank (Mantel–Cox) test, $n = 5$ mice per group in 2 independent experiments, $^{*}P < 0.0001$ vs *A. fumigatus* group. **c**, Phagocytic index calculated using the number of conidia that had

been phagocytosed for each macrophage (each point plotted is a cell). Fifty cells were counted for each data set in 2 independent experiments. The median, and the first and third quartiles of the distribution are represented in the box, with whiskers extending ±1.5× interquartile range, considering points outside as outliers. Statistical analysis was performed using two-sided one-way ANOVA (Bonferroni's test) for multiple comparisons. Line at mean, $*P < 0.01$, $**P < 0.0001$ vs *A. fumigatus* group. **d**, Conidia viability. BMDM cells were seeded at a density of 10^6 cells per ml and challenged with *A. fumigatus* conidia at an MOI of 1:10. After 24 h of incubation, media were removed and the cell suspensions were seeded in Sabouraud dextrose agar media. After 24 h of growth, the number of c.f.u.s ml^{-1} was evaluated. Data calculated using two-sided two-way ANOVA and subsequent Dunnett's multiple comparison test. Data are presented as mean ± s.d. from 3 biological replicates; $****P < 0.0001$ versus *A. fumigatus*. **e**, Percentage of acidified phagolysosomes (PLs) containing conidia. Data represent means ± s.d. of 3 biological replicates. *P* values were calculated using two-sided one-way ANOVA with Bonferroni's multiple comparisons test. NS, not significant. **f**–**i**, Cytokine production by BMDMs after infection with *A. fumigatus*, *A. fischeri*, *A. oerlinghausenensis* and *A. lentulus* conidia (MOI 1:10). Two-sided one-way ANOVA with subsequent Bonferroni's multiple comparison tests is shown for ELISAs. Data are presented as mean ± s.d. from 2 biological triplicates, with adjusted *P* values. $**P_{adj} < 0.0010$, $****P_{adj} < 0.0001$ vs *A. fumigatus*. ND, no data. **j**, Conidia internalization in A549 epithelial cells at 3 h post infection. Endocytosed conidia per HPF. Statistical analysis was performed using two-sided one-way ANOVA (Bonferroni's test) for multiple comparisons. Data are presented as mean ± s.d. from 3 biological duplicates. $**P_{adj} < 0.0014$. **k**, Damage to A549 epithelial cells as measured by specific ^{51}Cr release. Statistical analysis was performed using two-sided one-way ANOVA (Bonferroni's test) for multiple comparisons. Data are presented as mean ± s.d. from 3 biological duplicates. $*P_{adj} < 0.0265$, $****P_{adj} < 0.0001$.

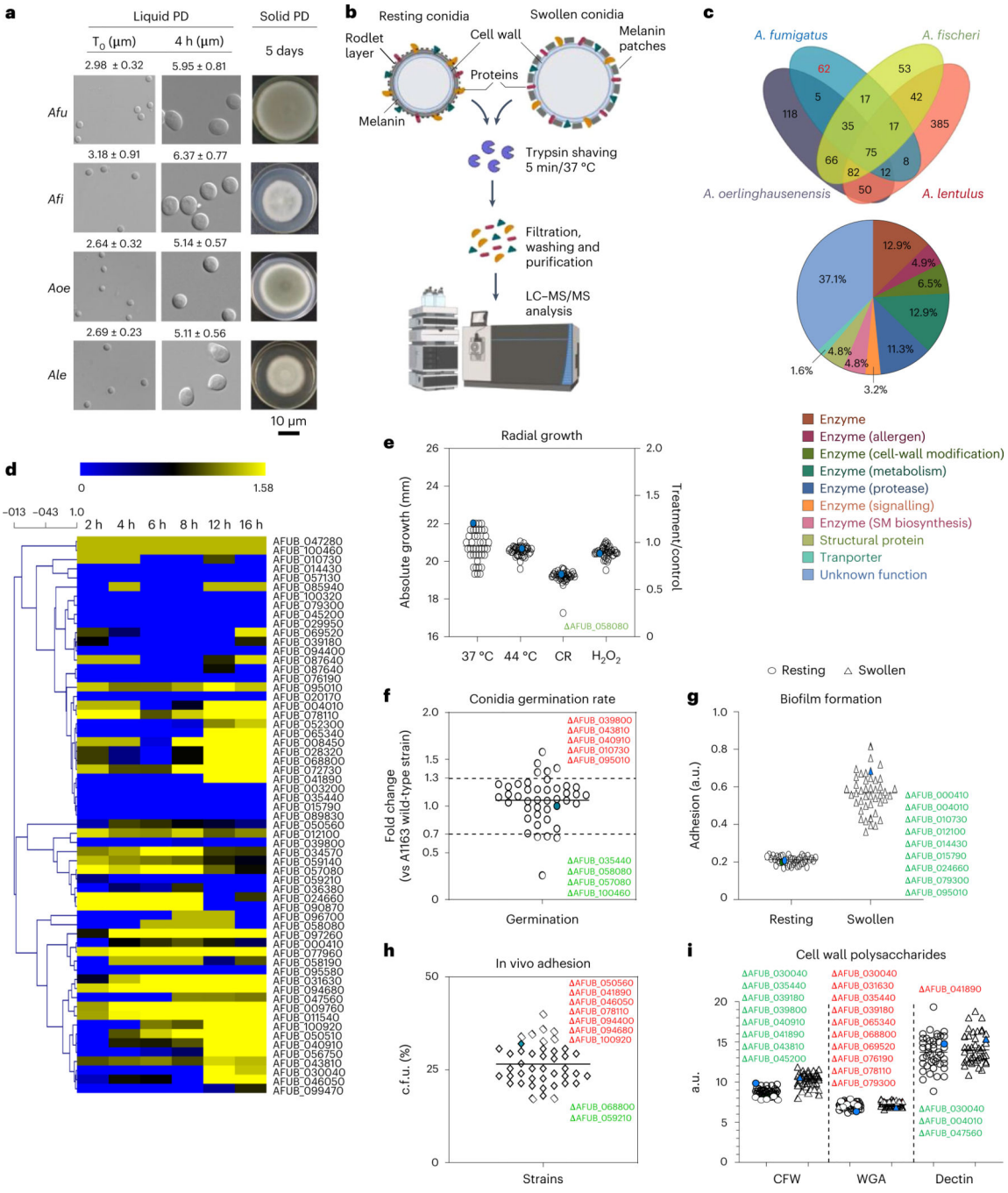

Fig. 2 |. Comparative trypsin-shaving proteomics to study the surface-associated proteome surfome of *A. fumigatus*.

a, Representative images of 3 different experiments showing *A. fumigatus*, *A. fischeri*, *A. oerlinghausenensis* and *A. lentulus* conidia at time 0 and 4 h post incubation at 37 °C (early germination) in liquid potato dextrose (PD) media and radial growth (10^4 conidia were displayed at the centre of MM plates and incubated for 5 days at 37 °C; radial diameters shown in Supplementary Table 8). **b**, Trypsin-shaving-based proteomic analysis workflow. Proteins obtained from trypsin-treated resting and swollen conidia were analysed by LC–

MS/MS. Created with BioRender.com. **c**, Sixty-two uniquely detected proteins constitute the *A. fumigatus* conidial surfome. The Venn diagram illustrates the intersection of proteins identified by trypsin shaving of resting and swollen conidia of *Aspergillus* spp. strains. The conidial surfome of *A. fumigatus* is composed of 62 uniquely detected proteins (in red). Functional categorization of the 62 proteins that comprise *A. fumigatus* surfome according to their description in FungiDB is also shown. **d**, Heat map of the mRNA accumulation (FPKM, fragments per kilobase of transcript per million fragments mapped) during conidial germination of 62 genes encoding the *A. fumigatus* surfome proteins. RNAseq database according to ref. 20. **e**, Growth phenotypes of the wild-type A1160 strain (in blue) and deletion strains grown for 72 h at 37 °C or 44 °C in solid MM and MM supplemented with Congo red (CR, 10 μg ml^{-1}) or hydrogen peroxide (H_2O_2, 1.5 mM). The results are the average of 3 biological repetitions. **f**, Germination rates of the wild-type A1160 strain (in blue) and deletion strains. Only those hits below or above the 30% fold-change threshold and statistically different from the parental strain A1160 are displayed in the figure. Results are the average of 3 biological repetitions. **g**, Adhesion, biofilm formation measured by CV assay, of resting (○) and swollen (Δ) conidia for all mutant strains and A1160 (in blue). The results are the average of 8 biological repetitions. **h**, In vivo adhesion assay with A549 pulmonary cells. **i**, Detection of chitin (CFW), *N*-acetylglucosamine (GlcNAc) (WGA) and β-(1,3)-glucan (Dectin) contents on the conidial surface of all mutant strains and A1160 (in blue) in resting (○) and swollen (Δ) conidia. The results are the average of 8 biological repetitions. Only hits that share the same significant phenotype (lower and higher detection in green and red, respectively) in both stages are highlighted in the figure. In the data in **e**–**i**, we have considered only the mutants that have 30% increase or decrease compared with the parental strain (A1163). Statistical analysis was performed using two-sided one-way ANOVA (Dunnett's test) for multiple comparisons. The selected mutants were significantly different from the A1163 wild type with $P \leq 0.05$.

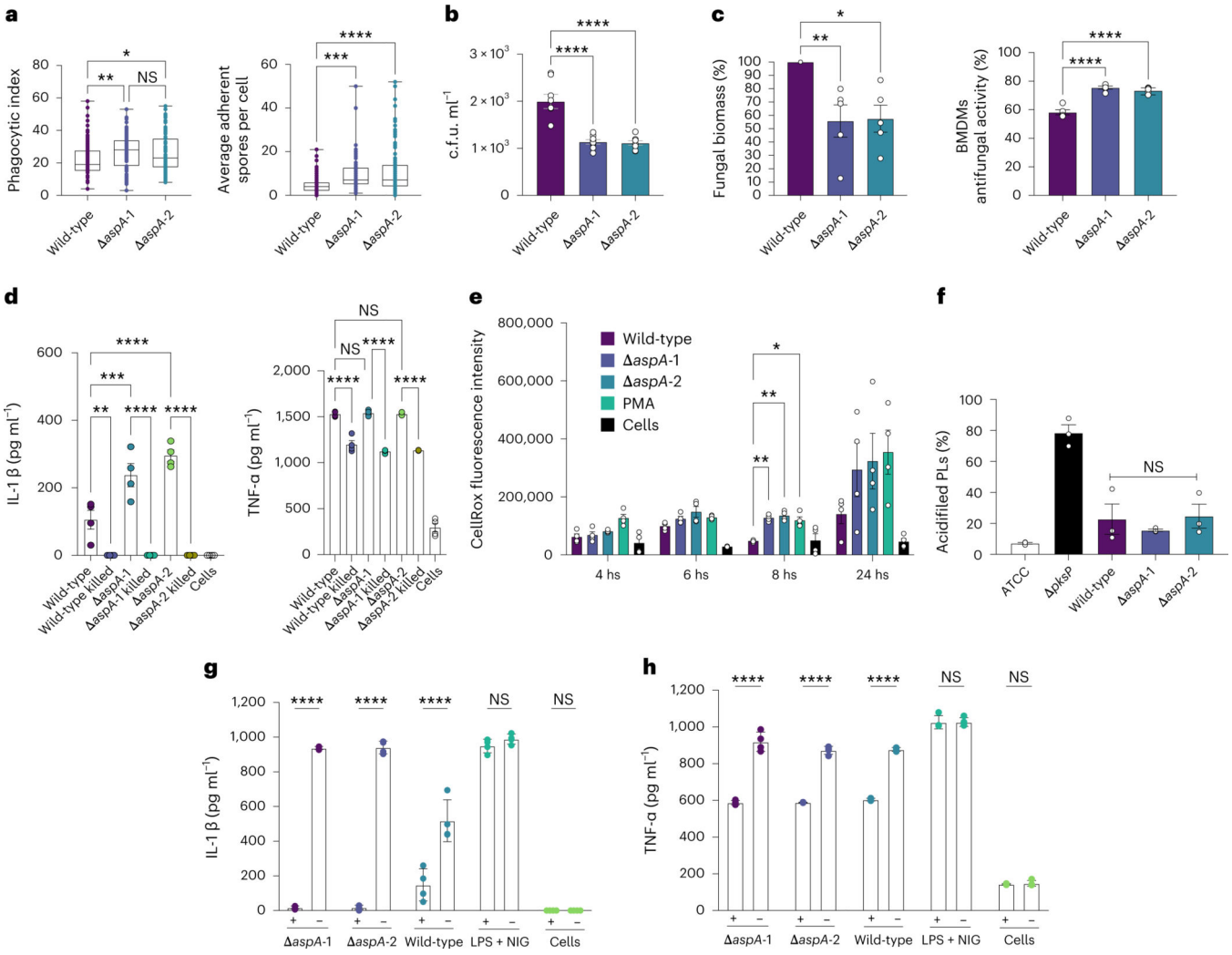

Fig. 3 |. The *A. fumigatus* Δ*aspA* mutant has reduced viability in the presence of BMDMs and can modulate IL-1β production.

a, The Δ*aspA* mutants have increased engulfment and adherence, and reduced viability in the presence of BMDMs compared with the wild-type strain. Phagocytic index (left) was calculated using the number of conidia that had been phagocytosed for each macrophage, and adherence (right) was calculated using the number of conidia counted in each macrophage surface (each point plotted is a cell). Fifty cells were counted for each data set in two independent experiments, totalling 100 cells. The median, and the first and third quartiles of the distribution are represented in the box, with whiskers extending to ±1.5× the interquartile range, considering points outside as outliers. Statistical analysis was performed using two-sided one-way ANOVA (Bonferroni's test) for multiple comparisons. *$P_{adj} < 0.0131$, **$P_{adj} < 0.0037$, ***$P_{adj} < 0.0002$ and ****$P < 0.0001$. **b**,**c**, BMDMs cells were challenged with *A. fumigatus* conidia at an MOI of 1:10. After 24 h of incubation, the cell suspensions were seeded and the number of c.f.u.s ml^{-1} (**b**) was evaluated. Statistical analysis was performed using two-sided one-way ANOVA (Bonferroni's test) for multiple comparisons. Data are presented as mean ± s.d. of 2 biological experiments with 3 replicates; ****$P < 0.0001$ vs A1163 wild-type strain. Fungal viability (**c**) upon 24 h

exposure to BMDMs as measured by MTT and CFW accumulation. Statistical analysis was performed using two-sided one-way ANOVA (Bonferroni's test) for multiple comparisons. Data are presented as mean ± s.d. of 5 independent biological repetitions. *$P_{adj} < 0.0128$, **$P_{adj} < 0.0100$ and ****$P_{adj} < 0.0001$ vs A1163 wild-type strain. **d**, UV-killed conidia show that Δ*aspA* conidia need to be alive to modulate IL-1β (left) and TNF-α (right) production. Statistical analysis was performed using two-sided one-way ANOVA (Tukey's test) for multiple comparisons. Data are presented as mean ± s.d. of 4 independent biological repetitions. **$P_{adj} < 0.0072$, ***$P_{adj} < 0.0007$ and ****$P_{adj} < 0.0001$. **e**, ROS accumulation upon exposure of the wild type and Δ*aspA* mutants to BMDMs in the indicated periods of time. PMA was used as a positive control for ROS induction. Statistical analysis was performed using two-sided one-way ANOVA (Dunnett's test) for multiple comparisons. Data are presented as mean ± s.d. of 3 independent biological repetitions. *P adj < 0,0267, **P adj < 0,0033. **f**, Percentage of PLs. Statistical analysis was performed using two-sided one-way ANOVA (Dunnet's test) for multiple comparisons. Data are presented as mean ± s.d. of 3 independent biological repetitions. **g**,**h**, Transwell migration assays. Wild type and Δ*aspA* mutants were exposed to BMDMs, and IL-1β and TNF-α production were measured. '+' and '−' indicate when the Transwell insert was added or not to the well plate, respectively. Results are the mean ± s.d. of 3 independent biological repetitions. Statistical analysis was performed using two-sided two-way ANOVA (Bonferroni's test) for multiple comparisons; ****$P < 0.0001$.

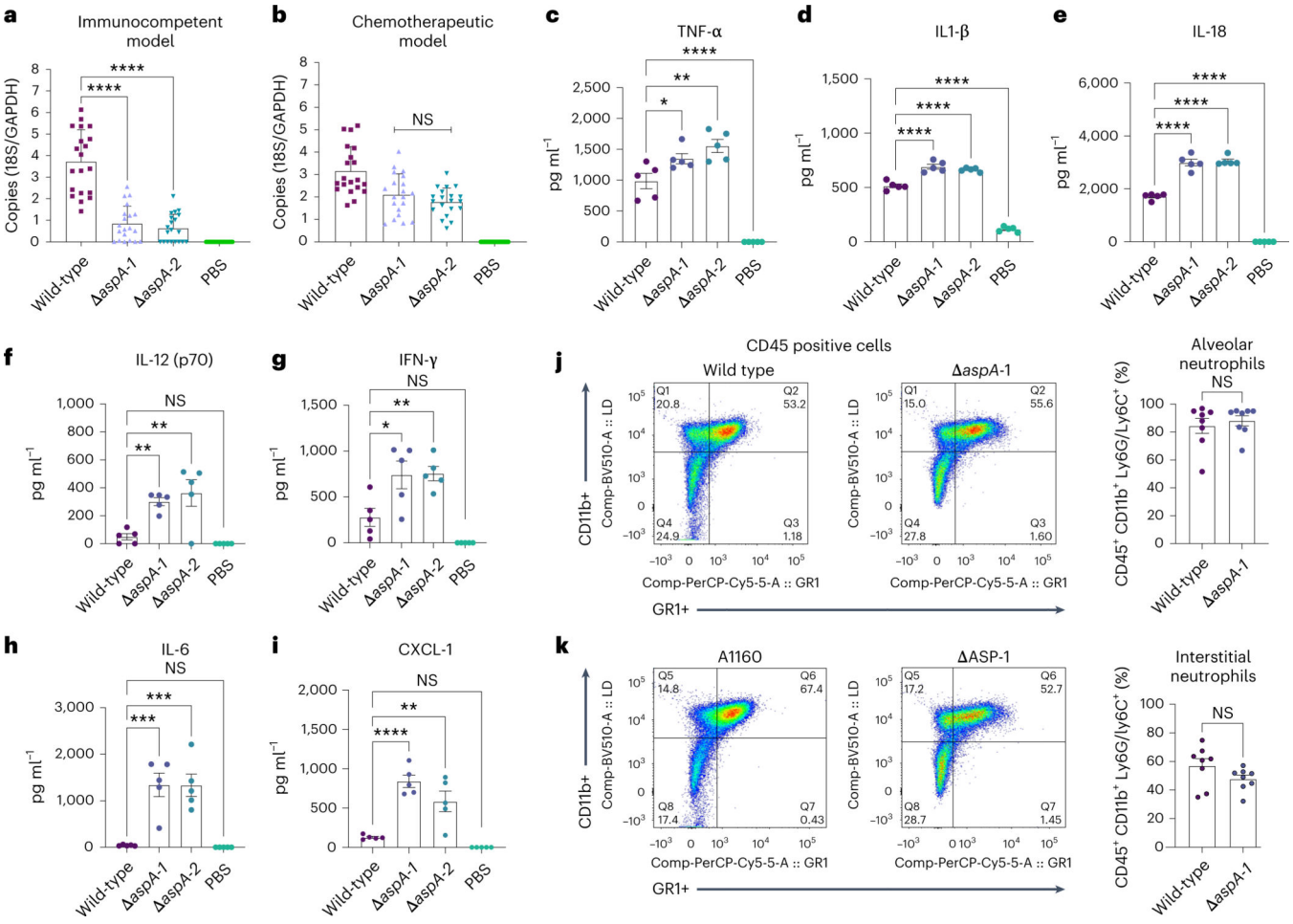

Fig. 4 |. Infection with *A. fumigatus* Δ*aspA* mutants results in decreased fungal burden in immunocompetent mice.

a, Fungal burden of the wild type and Δ*aspA* mutants in a murine chemotherapeutic mouse infection model. **b**, Immunocompetent mouse infection model. Statistical analysis was performed using two-sided one-way ANOVA (Dunnett's test) for multiple comparisons. Data are presented as values from $n = 10$ mice per group in two independent experiments. Results are the mean ± s.d. of 2 independent biological repetitions. **c**–**h**, Cytokine production (TNF-α, IL-1β, IL-18, IL-12, INF-γ and IL-6) in the immunocompetent mouse model infected with wild type and Δ*aspA* mutants. **i**, Chemokine production (CXCL-1) in the immunocompetent mouse model infected with wild type and Δ*aspA* mutants. The results graphic shows the mean ± s.d of 3–5 technical replicates. Statistical analysis was performed using two-sided one-way ANOVA (Dunnett's test) for multiple comparisons. For **a**–**i**, $*P < 0.05$, $**P < 0.01$, $***P < 0.001$, $****P < 0.0001$ vs the wild-type group. **j**,**k**, Fluorescence activated cell sorting (FACS) analysis of interstitial and alveolar neutrophils in mice infected with *A. fumigatus* wild-type and Δ*aspA-1* strains. A representative cytometry dot plot of $CD11b^+Ly6G^+/Ly6C^+$ cells gated from the $CD45^+$ population is shown from mice in each group. Data are presented as mean ± s.d of $n = 4$ mice per group in 2 independent experiments. The *P* values for the comparison between the groups were calculated using two-sided non-parametric *t*-test (two-tailed) with Mann–Whitney correction ($P > 0.05$).

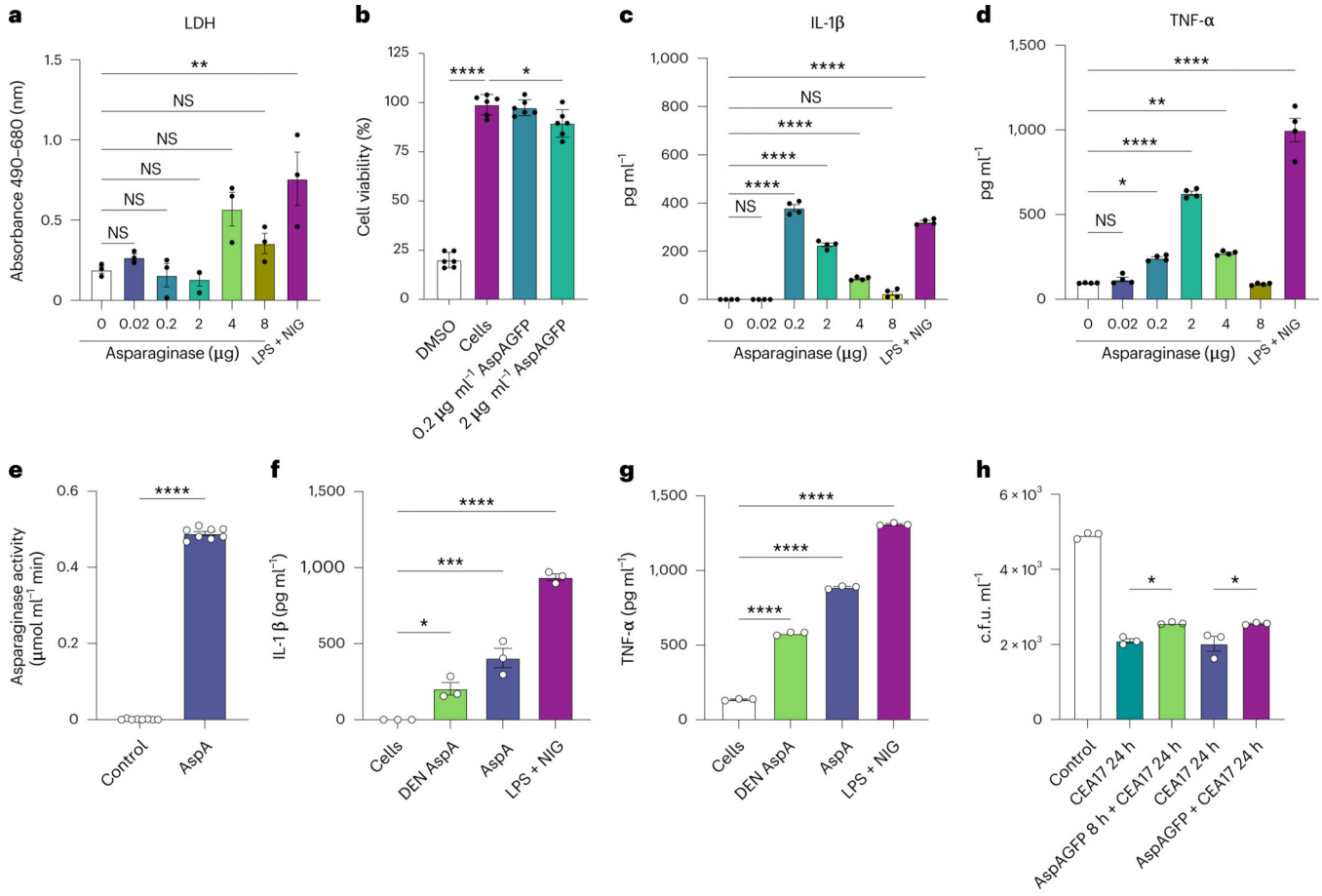

Fig. 5 |. Heterologously expressed AspA modulates IL-1β and TNF-α levels.

a, Viability of BMDMs exposed for 24 h at 37 °C to different concentrations of AspA and measured by LDH activity or **b**, exposed to DMSO, 0.2 or 2 μg AspA:GFP, and measured by XTT assay. In **a**, statistical analysis was performed using two-sided one-way ANOVA (Bonferroni's test) for multiple comparisons. Data are presented as mean ± s.d. of 3 biological experiments; $^{**}P < 0.0001$. In **b**, statistical analysis was performed using two-sided one-way ANOVA (Bonferroni's test) for multiple comparisons. Data are presented as mean ± s.d. of 5 biological experiments. $^{*}P_{adj} < 0.0148$, $^{****}P_{adj} < 0.0001$ vs DMSO. **c**,**d**, Increasing concentrations of AspA modulate IL-1β and TNF-α production by BMDMs. Statistical analysis was performed using two-sided one-way ANOVA (Bonferroni's test) for multiple comparisons. Data are presented as mean ± s.d. of 4 biological experiments; $^{*}P < 0.05$, $^{**}P < 0.01$, $^{****}P < 0.0001$. **e**, *A. fumigatus* AspA asparaginase activity. Data are presented as mean ± s.d. of 6 biological experiments; two-sided non-parametric *t*-test (two-tailed) was used for the statistical analysis; $^{****}P < 0.0001$. **f**,**g**, Denatured AspA triggers less IL-1β and TNF-α levels in BMDMs. Statistical analysis was performed using two-sided one-way ANOVA (Bonferroni's test) for multiple comparisons. Data are presented as mean ± s.d. of 3 biological experiments; $^{*}P < 0.05$, $^{***}P < 0.001$ and $^{****}P < 0.0001$. **h**, Conidial viability of BMDMs exposed or not to 2 μg AspA for 8 h and subsequent addition of conidia or 2 μg AspA together with conidia, evaluated after 32 and 24 h. Results are the average of 3 biological repetitions and are expressed as individual data points ±s.d.

Statistical analysis was performed using two-sided one-way ANOVA (Dunnett's test) for multiple comparisons; $*P < 0.05$.

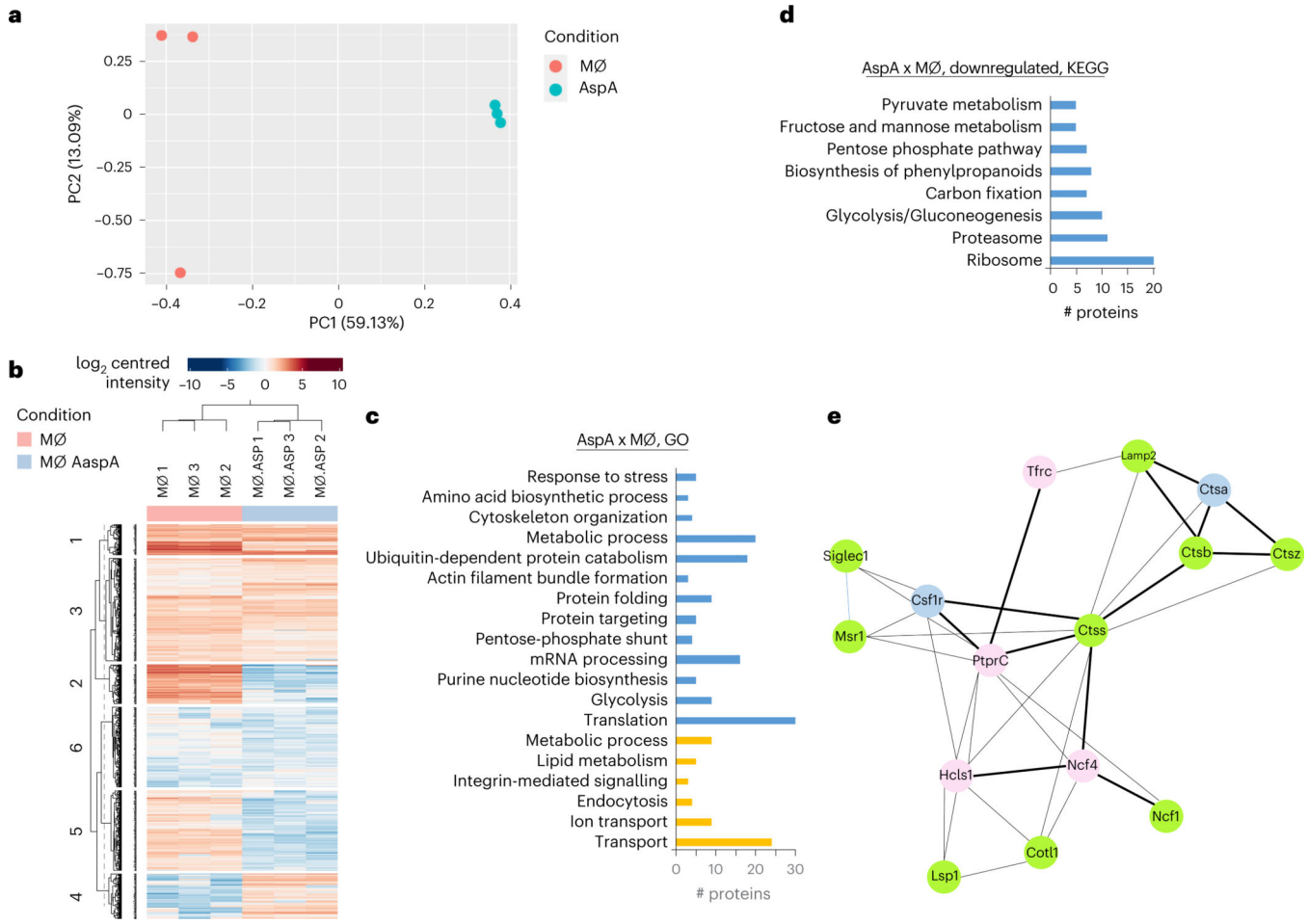

Fig. 6 |. Proteomic profiling of BMDMs exposed to AspA.

a, Principal component analysis distribution of 3 biological repetitions of BMDM and BMDM proteins exposed to AspA. **b**, Heat map of protein abundance of BMDM and BMDM exposed to AspA. **c**,**d**, Enriched categorization of BMDM and BMDM proteins exposed to AspA. Blue and pumpkin colours represent down- and up-expressed categories, respectively. All categories and *P* values are described in Supplementary Table 15. **e**, Mouse functional protein association network based on 15 selected proteins that are modulated in the BMDMs in the presence of AspA. Each node represents a protein that is differentially expressed in the BMDMs upon exposure to AspA. Each edge represents a functional protein association retrieved from the STRING (https://string-db.org) server (medium confidence threshold of 0.4 for the interaction score), and node sizes represent the number of edges connected to the node. Proteins were annotated on the basis of https://www.genecards.org and are: SIGLEC1, Msr1, Csf1r, TfrC, PtprC, Hcls1, Lsp1, Lamp2, Ctss, Ncf4, Colt1, CtsA, CtsB, CtsZ and Ncf1.